SEMMELWEIS EGYETEM

DOKTORI ISKOLA

Ph.D. értekezések

3512.

BERKI ÁDÁM JÓZSEF

Klinikai neurológiai kutatások
című program

Programvezető: Dr. Kovács Tibor, egyetemi tanár

Témavezető: Dr. Tamás Gertrúd, habilitált egyetemi docens

Modulation of Motor Network Dynamics by Subthalamic Stimulation in Parkinson's Disease

PhD thesis

Ádám József Berki, MD

Semmelweis University Doctoral College

János Szentágothai Neurosciences Division

Supervisor: Gertrúd Tamás, MD, PhD

Official reviewers: Annamária Juhász, MD, PhD
Boglárka Zsófia Hajnal, MD, PhD

Head of the Complex Examination Committee:
Dániel Bereczki, MD, DSc

Members of the Complex Examination Committee:
Andrea Kelemen, MD, PhD
Balázs Hangya, MD, DSc

Budapest
2026

Table of Contents

List of abbreviations

aDBS: adaptive deep brain stimulation
ANOVA: analysis of variance
ANT: Advanced Normalization Tools
cDBS: conventional deep brain stimulation
CSF: cerebrospinal fluid
DBS: deep brain stimulation
DLPFC: dorsolateral prefrontal cortex
EC: effective connectivity
ECoG: electrocorticography
EEG: electroencephalography
FEM: Finite Element Method
FTG: finely-tuned gamma
GM: gray matter
gPDC: generalized partial directed coherence
GPe: globus pallidus externa
GPi: globus pallidus interna
ICA: independent component analyses
IPG: implantable pulse generator
LCMV: linearly constrained minimum variance
LFM: lead-field matrix
LFP: local field potential
M1: primary motor cortex
MDS: International Parkinson and Movement Disorder Society
MEG: magnetoencephalography
MNI: Montreal Neurological Institute
MRI: magnetic resonance imaging
PAC: phase-amplitude coupling
PD: Parkinson's disease
PMC: premotor cortex
PSD: power spectral density

ROI: region of interest

S/m: siemens per metre

SD: standard deviation

SHAP: Kernel SHapley Additive exPlanations

SMA: supplementary motor area

SNc: substantia nigra pars compacta

SNr: substantia nigra pars reticulata

SPM: Statistical Parametric Mapping

STN: subthalamic nucleus

SVM: support vector machine

TBT: technology-based tool

UPDRS: Unified Parkinson's Disease Rating Scale

VC: visual cortex

WM: white matter

1. Introduction

1.1. Bradykinesia and Parkinson's disease

Parkinson's disease (PD) is the second most prevalent neurodegenerative disorder of the central nervous system, characterized by a chronic and progressively disabling combination of motor and non-motor symptoms (1). Of the four cardinal features (bradykinesia, postural instability, rigidity, and resting tremor), bradykinesia is the core symptom for the diagnosis of PD, and it is a key contributor to deterioration in quality of life (2, 3). The Movement Disorders Society and the United Kingdom Parkinson's Disease Society Brain Bank currently define bradykinesia in PD as slowness of movement accompanied by a decrement in the speed or amplitude of successive movements (4, 5).

1.1.1. Pathophysiology and neural signatures of bradykinesia

In the classical firing-rate model, bradykinesia has been attributed to deficient information processing within the basal ganglia circuitry (6). In the basal ganglia-thalamocortical loop, the striatum is the principal input zone, receiving projections from multiple cortical areas, the intralaminar thalamic nuclei, and the substantia nigra pars compacta (SNc). The globus pallidus interna (GPi) and substantia nigra pars reticulata (SNr) function as output nuclei, exerting a net inhibitory effect on thalamocortical activity. Three parallel pathways mediate information transmission in the basal ganglia. In the direct pathway, striatal medium spiny neurons directly inhibit the GPi, thereby promoting movement initiation. In the indirect pathway, striatal medium spiny neurons block inhibitory input from the globus pallidus externa (GPe) to the subthalamic nucleus (STN), thereby activating the GPi/SNr complex and resulting in overall inhibition of movement. The third stream is a hyperdirect, monosynaptic, excitatory, and bidirectional connection between the motor cortex and the STN, mediating rapid action suppression (7). Dopamine facilitates movement by activating excitatory D1 receptors in the direct pathway and inhibiting D2 receptors in the indirect pathway. In PD, dopaminergic denervation of the striatum decreases the firing rate of direct pathway neurons. In contrast,

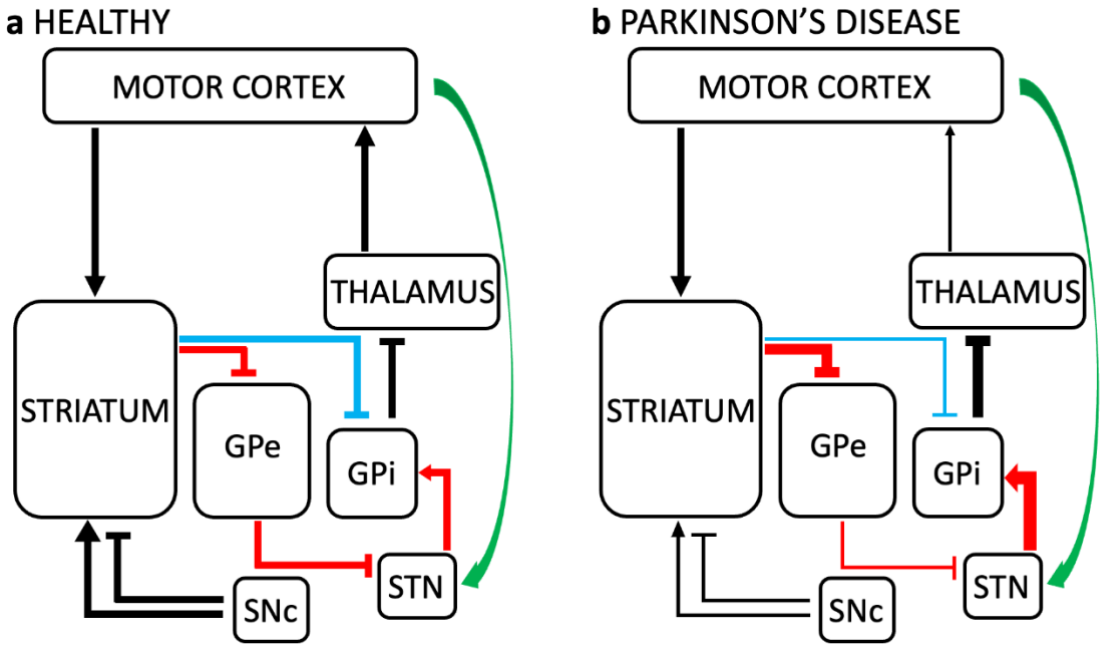

Figure 1. Basal ganglia circuits under (a) normal physiological conditions and (b) in Parkinson's disease Degeneration of dopaminergic input from the substantia nigra pars compacta (SNc) leads to alterations in neuronal firing across downstream nuclei. This ultimately results in increased inhibition of thalamic signals projecting to the cortex. In the diagram, increased firing rates are shown with thicker lines, whereas thinner lines represent decreased activity. Excitatory pathways are illustrated with arrows, while inhibitory pathways terminate in flat bars. The indirect pathway is highlighted in red, the direct pathway in blue, and the hyperdirect pathway in green. GPe (globus pallidus externa), GPi (globus pallidus interna), SNr (substantia nigra pars reticulata), and STN (subthalamic nucleus)

neurons in the indirect pathway are released from inhibition, resulting in excessive suppression of thalamocortical and corticospinal motor pathways (2, 8) (Figure 1). However, based on current neuroanatomical evidence, the firing rate model cannot fully account for bradykinesia, and coherent oscillatory activity of the entire basal ganglia-thalamocortical loop must be considered to understand the bradykinesia complex (2).

Apart from static changes in firing rate, dynamic alterations in bursting activity and synchronization patterns of basal ganglia neurons have been observed (9).

Local field potential (LFP) recordings from the STN or GPi can be obtained intraoperatively (10), in the postoperative phase via externalized deep brain stimulation

(DBS) electrodes (11), or in the chronic phase of DBS through sensing electrodes (12). Physiological beta band (13–35 Hz) activity in the basal ganglia, occurring in transient bursts, is thought to facilitate motor planning, executive processing, movement accuracy (9), and motor response inhibition during behavioral processes (13). However, in Parkinson's disease, previous studies have found that excessive beta band oscillatory activity is a signature of dopamine-denervated network elements (14-17). This enhanced beta band rhythm is characterized by bursts of increased duration and amplitude (18), predominantly involving indirect pathway neurons (19).

Intraoperative recordings from patients undergoing DBS surgery revealed a significant correlation between subthalamic beta band power (13–30 Hz) (20), burst duration, and bradykinesia severity (21). Beta band oscillations in the dorsal pallidum also scaled with the velocity during a simple pressing task (21). Within the STN, a combined tractography and LFP study localized beta activity to the dorsolateral subthalamic nucleus (22).

Furthermore, distinct roles of beta sub-bands have been identified: while low beta activity in the STN reacts actively to levodopa intake (23) and DBS (17), high beta activity operates along the hyperdirect pathway between the STN and the primary motor cortex (M1) (16, 24) premotor cortex (PMC) (17), and supplementary motor area (SMA) (16, 17, 25) and responds to stimulation adjustment (26). Excessive broadband beta activity in relation to bradykinesia has also been observed in the motor cortex using electrocorticography (ECoG) (27) and electroencephalography (EEG) (28).

Beyond beta frequency, gamma oscillations in the STN (29), GPi (30), and motor cortex (31) underlie adequate movement execution and are involved the monitoring of ongoing movements. Two types of gamma activity have been identified across the basal ganglia-thalamocortical circuit. A broader range of oscillations (30–105 Hz) has been described, emerging within the basal ganglia during movement and subsiding in the resting state (32); such subthalamic broadband gamma rhythm in PD patients scales with the amplitude and speed of voluntary hand movements and negatively correlates with reaction time (33). A narrower-band gamma rhythm (60–90 Hz), termed finely-tuned gamma (FTG), develops in the awake state within the pedunculopontine nucleus as part of the ascending reticular activating system and is streamed to the basal ganglia and motor cortex through direct afferents; it further increases before and during voluntary movement execution, determining its speed, amplitude, and force (34). A decreased dopamine level

is associated with reduced subthalamic FTG activity, whereas levodopa administration increases its power, in parallel with improved motor performance (35). Intraoperative subthalamic microelectrode recordings showed that FTG is spatially limited to the dorsolateral part of the STN and exhibits a phase lead over motor cortical FTG oscillations (16).

Previous studies have primarily examined the neural basis of bradykinesia using simple motor tasks (36-38). Modeling everyday multi-joint movements, such as drawing or handwriting, has been proposed to yield more information about the pathophysiology of the cortico-basal ganglia network (39). However, the network-level changes induced by DBS during complex graphomotor tasks have not yet been described.

Concurrently, combined testing methods were applied to measure activity from different subcortical and cortical network elements. Perioperative measurements of subthalamic local field potentials, in combination with implanted ECoG strips above restricted motor cortex areas (24) or EEG (16, 40)/magnetoencephalography (MEG) (15, 17, 23, 25, 41), are affected by the stun effect (25). Subthalamic local field potentials have been measured using externalized leads in the chronic phase during the replacement of the impulse generator (36, 42) or by chronically implanted sensing stimulators (20); however, cortical activity during these measurements was not assessed. Indeed, EEG is a safe method and can be used in many patients who are chronically stimulated, also with non-sensing impulse generators. In this way, the changes in the subthalamic-cortical connections and the intercortical processes can be mapped in detail.

1.1.2. Measurement methods of bradykinesia

Evaluation tools of motor performance include clinical rating scales and technology-based assessments. At present, the gold-standard clinical scales are the Unified Parkinson's Disease Rating Scale (UPDRS) (43) and its revised form updated by the International Parkinson and Movement Disorder Society (MDS): MDS-UPDRS (44). The motor section of the scale (part III) provides instructions for quantifying upper- and lower-limb bradykinesia, and has demonstrated high reliability in previous studies (45). However, items such as finger tapping or pronation-supination of the hands are the most difficult to rate on a 0 (normal) to 4 (severe) scale. They are prone to inter- and intra-rater

variability (45). Moreover, in the aforementioned scales, movement speed, amplitude, and rhythm cannot be rated separately, but the same score may represent different facets of motor impairment (46). When evaluating the reliability of UPDRS scores, some studies found low inter-rater variability (47). In contrast, others demonstrated substantial variability and poor overall agreement when evaluating the hand movements of PD patients (48). It was also reported that mild motor impairments are more difficult to rate precisely (49).

Technology-based tools (TBTs) provide objective assessments of movement and are more sensitive to subtle changes in motor performance, improving intra- and inter-rater reliability (50). These include uniaxial and triaxial accelerometers measuring linear acceleration (51), gyroscopes assessing angular velocity (52), and magneto-inertial sensors integrating a three-axis accelerometer, a gyroscope, and a magnetometer to measure motion and orientation in three-dimensional space (53). Some of these sensors also enable the collection of real-world kinematic data in home-based environments using wearable devices (54), computers (55), or smartphone applications (56). The majority of the tools measure simple repetitive limb movements, while others yield information on complex, multi-joint motor activity.

Spiral drawing analysis previously showed that linear parameters, including drawing speed, first-order zero crossing, and second-order smoothness, are markers of disease severity (57), correlate with the motor section of the MDS-UPDRS-III (58), and may capture subtle kinematic changes beyond the sensitivity of the UPDRS-III (57, 59). Spiral drawing may represent a practical and sensitive tool for monitoring both disease progression (60) and the effects of STN stimulation in the postoperative phase (61). Altogether, while rating scales offer standardized measures of symptom severity and functional impairment, TBTs can capture more detailed, real-time changes in motor performance. More precise monitoring could support better-informed clinical decisions and the development of treatment plans that are tailored to the patient's specific needs, ultimately improving overall disease management and quality of life.

1.2. Deep brain stimulation for Parkinson's disease

1.2.1. Role, indication, patient selection, and target points

Deep brain stimulation (DBS) is a functional neurosurgical therapy that modulates neural activity through electrical stimulation of specific brain regions (62). Its advantages include selective targeting, adjustable stimulation parameters tailored to clinical response, continuous therapeutic effect over 24 hours, and reversibility without causing permanent tissue damage (63). Large clinical studies have demonstrated that DBS is more effective than medication alone in alleviating both core motor and non-motor symptoms (63), while also enhancing quality of life in patients with advanced Parkinson's disease (64), as well as in patients at earlier stages experiencing troublesome motor fluctuations (65). Current indications include persistent motor fluctuations in advanced disease, early but disabling fluctuations, and medication-resistant tremor (66).

Successful outcomes of DBS therapy depend on careful patient selection, and several factors must be considered in clinical practice. A Delphi expert consensus panel defined advanced Parkinson's disease as patients meeting the 5-2-1 criteria — taking levodopa ≥5 times daily yet experiencing ≥2 hours of "off" time and ≥1 hour of troublesome dyskinesia per day — and exhibiting significant impairment in activities of daily living (67). DBS shows consistent efficacy in large-scale multicenter trials in the advanced stages of Parkinson's disease, especially for patients experiencing motor fluctuations and dyskinesias inadequately controlled with medication (68). Age has been found to correlate negatively with postoperative outcome; however, functional status outweighs chronological age (69). Patients with advanced PD undergoing DBS surgery have an average disease duration of 12–15 years (66). Patients aged 75 years or older have a risk of complications in the first three postoperative months similar to that of younger patients (70); however, most DBS centers preferentially select candidates younger than 70–75 years (71). Based on the EARLY-STIM trial, DBS is now offered to patients with a disease duration of at least four years who have troublesome motor fluctuations despite adequate dopaminergic treatment (65).

Recommended preoperative evaluations include physical examination, levodopa challenge test, assessed with the UPDRS or MDS-UPDRS scales, cranial MRI (or CT

when MRI is contraindicated), neuropsychological assessment to identify dementia, cognitive dysfunction, personality and behavioral disorders or psychotic symptoms, as well as a patient diary, documenting motor states over at least 24 hours in 30-minute intervals, including periods of ON, ON with mild dyskinesia, ON with severe dyskinesia, OFF, and sleep (72). The Levodopa challenge test consists of administering a single suprathreshold dose of levodopa in the morning after a 12-hour withdrawal from antiparkinsonian medication (73). An improvement of at least 30% in the UPDRS or MDS-UPDRS motor score is used to predict a favorable short-term motor response (74). However, recent evidence suggests that the long-term outcome of DBS implantation does not relate to pre-surgical levodopa responsiveness, and the primary aim of the test is to identify non-responders. In cases of drug-resistant tremor, the response to levodopa is not indicative (71).

Potential DBS targets are the STN, GPI, and ventral intermediate nucleus (Vim) of the thalamus. STN DBS leads to substantial improvements in bradykinesia, rigidity, tremor, and difficulty initiating movement. The duration of the ON phase can increase by around six hours on average, while the OFF phase may decrease by 50–70% (63). Dopaminergic medication doses can be reduced by about half, thereby diminishing levodopa-induced involuntary movements, dopamine dysregulation syndrome, and impulse control disorders (69). Gait freezing, sleep, pain, and fatigue may also improve (75). However, postural instability and speech difficulties may worsen (69). Long-term follow-up studies spanning the first decade after implantation have demonstrated that the therapeutic benefits of subthalamic stimulation can persist (76).

GPi DBS has proven effective in reducing hyperkinesia, but usually does not result in a significant reduction in the dosage of dopaminergic medications. Its efficacy in alleviating rigidity and bradykinesia appears comparable to that of subthalamic nucleus stimulation, and it is less likely to cause balance problems, cognitive decline, or mood impairment (77). Vim stimulation selectively reduces tremor by approximately 70% and is sometimes used in combination with GPi DBS (71).

1.2.2. Neurobiology of deep brain stimulation in Parkinson’s disease

Understanding the effects of DBS requires a clear characterization of the electric field generated. DBS consists of three main implanted components: electrodes (leads), an extension wire, and a battery-powered implantable pulse generator (IPG) in the chest. DBS leads are designed with different contact numbers, contact lengths, and intercontact spacing. Standard DBS leads are quadripolar electrodes that produce a roughly spherical or cylindrical electrical field. More advanced designs, such as directional electrodes and multi-electrode configurations, allow for more precise shaping and targeting of the stimulation field. The electrode is composed of platinum-iridium wires, chosen for their low toxicity and excellent electrical conductivity. The stimulation electrode delivers pulsatile electrical currents through an active contact configured as the cathode. The anode can be assigned either to the IPG (monopolar configuration) or to a separate contact on the same electrode (bipolar configuration). The pulse shape is rectangular and pseudo-monophasic, consisting of a high-amplitude "active" phase followed by a low-amplitude, long-duration "passive" recharging phase to balance charge and prevent tissue damage. Stimulation settings are typically programmed within a frequency range of 130–180 Hz, with pulse widths of 30–200 μs, and amplitudes of approximately 0.7–4 mA or 1–5 V (78).

The effect of stimulation also depends on the targeted neural circuits and synapses. To this end, DBS exerts its strongest effects on larger, myelinated axons, triggering action potentials on both target afferent (antidromically, i.e., back towards the afferent neuron) and efferent fibers (orthodromically, i.e., downstream effect) (78). In the subthalamic nucleus, approximately 60% of afferents are inhibitory GABAergic inputs from the external globus pallidus (GPe). In comparison, the remaining ~40% are excitatory glutamatergic projections primarily from the cortex, reflecting the prominent contribution of the cortico-subthalamic hyperdirect pathway (79). Activation of STN afferents by DBS results in a net inhibitory effect, suppressing subthalamic neuronal firing rate. Similarly, GPi stimulation hyperpolarizes pallidal neurons, which receive predominantly GABAergic inputs (80).

Beyond firing-rate modulation, DBS induces changes in LFP dynamics. LFPs are thought to arise from the collective summation of excitatory and inhibitory postsynaptic currents, providing a mesoscopic readout of network activity (81). Simultaneous STN-LFP and MEG recordings have shown that, in the hypodopaminergic state, physiological

hyperdirect high beta activity (21–35 Hz) may lead to the emergence of pathological low beta synchrony (13–20 Hz) within the basal ganglia, accompanied by abnormally enhanced cortico-subthalamic coherence (reflecting the constant phase relationship of oscillatory components) (25). With sustained high-frequency stimulation, excitatory cortical inputs to the STN become progressively attenuated, leading to cortico-subthalamic decoupling and a concomitant suppression of pathological beta band activity in both subthalamic and cortical networks (82). On the other hand, broadband cortical gamma synchronization [35–100 Hz (28, 83), 50–200 Hz (84, 85), or even 300–400 Hz (86)] involving the primary motor cortex is enhanced during movement (83, 84) and DBS (28), suggesting a compensatory role against dopamine deficiency.

Narrow-band, finely tuned gamma (FTG) activity (60–90 Hz) is coherent in the STN and sensorimotor cortex (35, 86) and increases after levodopa intake (40, 86) or STN stimulation (87); it increases further with voluntary movements (86). Investigations of stimulation-related changes in the low and high beta and gamma bands are restricted in (28) extended motor cortex regions.

Previous studies have also reported excessive beta-gamma cross-frequency phase-amplitude coupling (PAC) within various anatomical hubs of the motor network and between them (88). Subthalamic stimulation reduced activity in the low beta band−(100–400 Hz) (89) within the STN, in the broad beta−[50–150 (90)/200 (91) Hz] ranges within the motor cortical areas; however, it has not yet been examined along the STN-motor cortex pathways.

1.2.3. Current technologies and future directions

Conventional deep brain stimulation (cDBS) delivers continuous electrical stimulation using preconfigured parameters (92). Temporal fluctuations in symptom severity during ON and OFF states may lead to periods of understimulation or overstimulation, worsening core symptoms and side effects (93). Both STN and GPI cDBS can induce dysarthria, paresthesia, ocular deviation, gait disturbance, dyskinesia, muscle contractions, or dystonic posturing (94). Technological advances in DBS engineering have enabled more individualized treatment strategies and reduced stimulation-induced side effects (95). In particular, directional leads allow current steering to selectively target

therapeutically relevant subregions, thereby improving the therapeutic window and reducing stimulation of adjacent structures associated with adverse effects. At the same time, closed-loop or adaptive DBS (aDBS) systems use physiological biomarkers to dynamically adjust stimulation amplitude in response to fluctuations in neural state (93). Most adaptive DBS (aDBS) studies have used the spectral power of the subthalamic beta band (13–30 Hz) rhythm as the control signal, as it positively correlates with the severity of bradykinesia and rigidity (96). Currently, two main adaptive algorithms are used in clinical studies. Single-threshold algorithms rapidly adjust stimulation in response to short bursts of pathological beta activity, directly targeting abnormal neural dynamics (97). Dual-threshold algorithms respond to slower trends in beta activity using upper and lower thresholds corresponding to OFF and ON states (98). While single-threshold systems are more sensitive to pathological bursts, dual-threshold systems provide smoother, more stable feedback. Beta-driven aDBS has shown that stimulation output can decrease during periods of peak levodopa effect while maintaining therapeutic benefit (99). Studies have also reported favorable effects on speech and reductions in troublesome dyskinesia compared to cDBS (100). However, several limitations must be considered when using a beta-based control signal. First, beta activity is strongly influenced by voluntary movements (26). Second, DBS suppresses STN beta activity even at low therapeutic amplitudes, which may confound its use as a biomarker of residual motor impairment (20, 26). Third, beta band signals may be contaminated by stimulation artifacts during simultaneous sensing and stimulation, particularly when recorded from adjacent or nearby contacts (96). On the other hand, stimulation-entrained gamma oscillations in the STN and motor cortex (60–90 Hz) were identified as an optimal biomarker for symptom control (100), highlighting the value of multi-site brain recordings in developing effective aDBS algorithms.

2. Objectives

In our present study, we examined patients with Parkinson's disease in the chronic phase after STN DBS surgery using a 64-channel EEG while they performed traced and self-paced complex hand movements with their more-affected hand under different levels of contralateral stimulation. We investigated how cortico-subcortical network activity is influenced by adjusting stimulation intensity during traced and self-paced spiral drawings. To this end, the specific objectives are as follows:

1. To determine the effect of ramping stimulation on spiral drawing parameters.

2. To identify motor subnetworks using an EEG-based source estimation technique whose stimulation-dependent activity may predict the improvement of bradykinesia during complex hand movements.

3. To explore stimulation- and task-related reactions in frequency-specific connectivity between the subnetwork elements.

Together, these objectives aim to elucidate how multiplex activity feature perception of complex network dynamics might accurately predict bradykinesia in Parkinson's disease.

3. Methods

3.1. Study participants and protocol

Thirty-eight patients diagnosed with idiopathic Parkinson's Disease and treated with bilateral STN-DBS for at least 1 year were recruited at the Department of Neurology, Semmelweis University, Hungary. The patients signed an informed consent form in accordance with the Declaration of Helsinki. The Medical Research Council in Hungary has provided ethical approval (080958/2015/OTIG) for the study. Inclusion criteria were bradykinesia and rigidity as leading symptoms. Candidates previously diagnosed with musculoskeletal disorders or dementia were excluded from the study. Motor performance was assessed using the Hoehn and Yahr Scale and the UPDRS part III. We converted the preoperative MDS-UPDRS part III scores in 2/38 patients and the postoperative scores in 10/38 patients to the UPDRS part III scores (101). All dopaminergic medications were only stopped 12 hours before the test because patients did not tolerate the discomfort. The study protocol is summarized in Figure 2.

3.2. Surgical procedure

Bilateral DBS leads (in 21 patients: Medtronic 3389; 9 patients: St Jude 6147; 7 patients Abbott 6170; 1 patient: Boston 2202) were implanted using standard stereotactic procedures (102) with the aid of microelectrode recording and clinical testing. Impulse generators were connected on the same day. For individualized anatomical planning, stereotactic contrast-enhanced CT imaging was obtained on the day of surgery with a Leksell G Frame fixed to the patient's head. Preoperative targeting and trajectory planning were performed using Medtronic FrameLink 5. Preoperative MRI data, consisting of contrast-enhanced three-dimensional T1-weighted images with 1-mm slice thickness and T2-weighted images with 2-mm slice thickness, were acquired on a Philips Achieva 3T MRI within six months before surgery. These MRI datasets were subsequently co-registered with the stereotactic CT images. The individual anatomical target within the Subthalamic Nucleus was determined according to established stereotactic guidelines (103). Specifically, the target point was positioned 3 mm lateral to

the intersection of the anterior and lateral borders of the Red Nucleus at its maximal diameter. Electrode trajectories were selected based on each patient's individual anatomical configuration. Dopaminergic medication was discontinued 12 hours before the procedure. Intraoperative electrophysiological mapping was performed with five microelectrodes, and clinical responses were evaluated by macrostimulation.

Lead implantation was performed under local anesthesia, whereas IPG implantation was performed under general anesthesia. Fluoroscopic guidance was used to assist electrode placement. Six weeks after surgery, postoperative contrast-enhanced CT scans with a 1-mm slice thickness were obtained. These CT images were fused with the preoperative MRI data using Medtronic FrameLink 5, and the accuracy of image registration was verified at multiple anatomical levels. CT images were thresholded to retain only the electrode contacts. The distal end of the first contact (contact 0) and the center of a proximal contact were selected to perform three-dimensional Euclidean vector calculations. Based on these calculations, the positions of the active contacts were estimated at distances of 0.75, 2.75, 4.75, and 6.75 mm, and their anatomical relationship to the Subthalamic Nucleus was visually confirmed on T2-weighted MRI sequences. For both hemispheres, the most distal electrode contact was designated contact 0, and the most proximal contact was labeled contact 3. The patients had no surgical or hardware-related complications in the perioperative phase.

3.3. Electrode localization

The DBS electrode localization of all patients was determined using the default settings of an advanced processing pipeline in the Lead-DBS software, version 3.1 (https://www.lead-dbs.org/) (104). Our approach involved linear co-registration of post-operative head CT or MRI scans to pre-operative T1-weighted images using Advanced Normalization Tools (ANTs; http://stnava.github.io/ANTs/) (105). Co-registration results were corrected for potential intra-operative brain shift using an automated subcortical refinement module within Lead-DBS. We used the STN atlas definitions from the DBS Intrinsic Template atlas, version 1.1 (106), for all analyses and visualizations. This precise subcortical atlas was explicitly created for use within Lead-DBS and is based on multi-

modal MRI, histology, and structural connectivity information. Normalization warp fields were manually refined using the WarpDrive toolbox (107) included in Lead-DBS, version 3.1 (108), to further enhance registration accuracy. Special attention was given to any visible mismatches in the registration, particularly focusing on the STN as the anatomical structure of interest. The integration of patient-specific active electrode contacts with corresponding stimulation parameters was simulated using an adaptation of the SimBio/FieldTrip pipeline (https://www.mrt.uni-jena.de/simbio/ and http://fieldtriptoolbox.org/) (109), as implemented in Lead-DBS, version 3.1 (104). Finally, we computed the Euclidean distance between the active contact points and the center of the STN motor segment.

3.4. Prescreening

A prescreening with the Kinesia motion capture system (Great Lakes Neurotechnologies Inc., USA) assessed the kinematic parameters of finger tapping, hand grasping, and pronation-supination of the most affected hand, the day before the primary measurement. The contralateral DBS lead was turned off for 1 h, and the patients performed each task for 15 s and then repeated the tasks after elevation of stimulation intensity with 0.5 V/mA steps until the level produced the best improvement without provoking side effects. Kinesia speed, amplitude, and rhythm subscores were calculated for each patient and on each stimulation level (49, 110). We determined the total Kinesia scores (0–4) out of the subscores by combining the three hand movement tasks (111). Using the total Kinesia scores, we selected four distinct levels of contralateral stimulation: 0 (OFF state), 1 (mild improvement), 2 (moderate improvement), and 3 (maximum improvement without side effects). The clinically most effective contact location was used for test stimulation throughout the study, during 12-h medication withdrawal. We applied the clinically most effective stimulation configuration, which was unipolar in all patients. Stimulation intensity in Volts was converted to current intensity (mA) based on the individual impedance values.

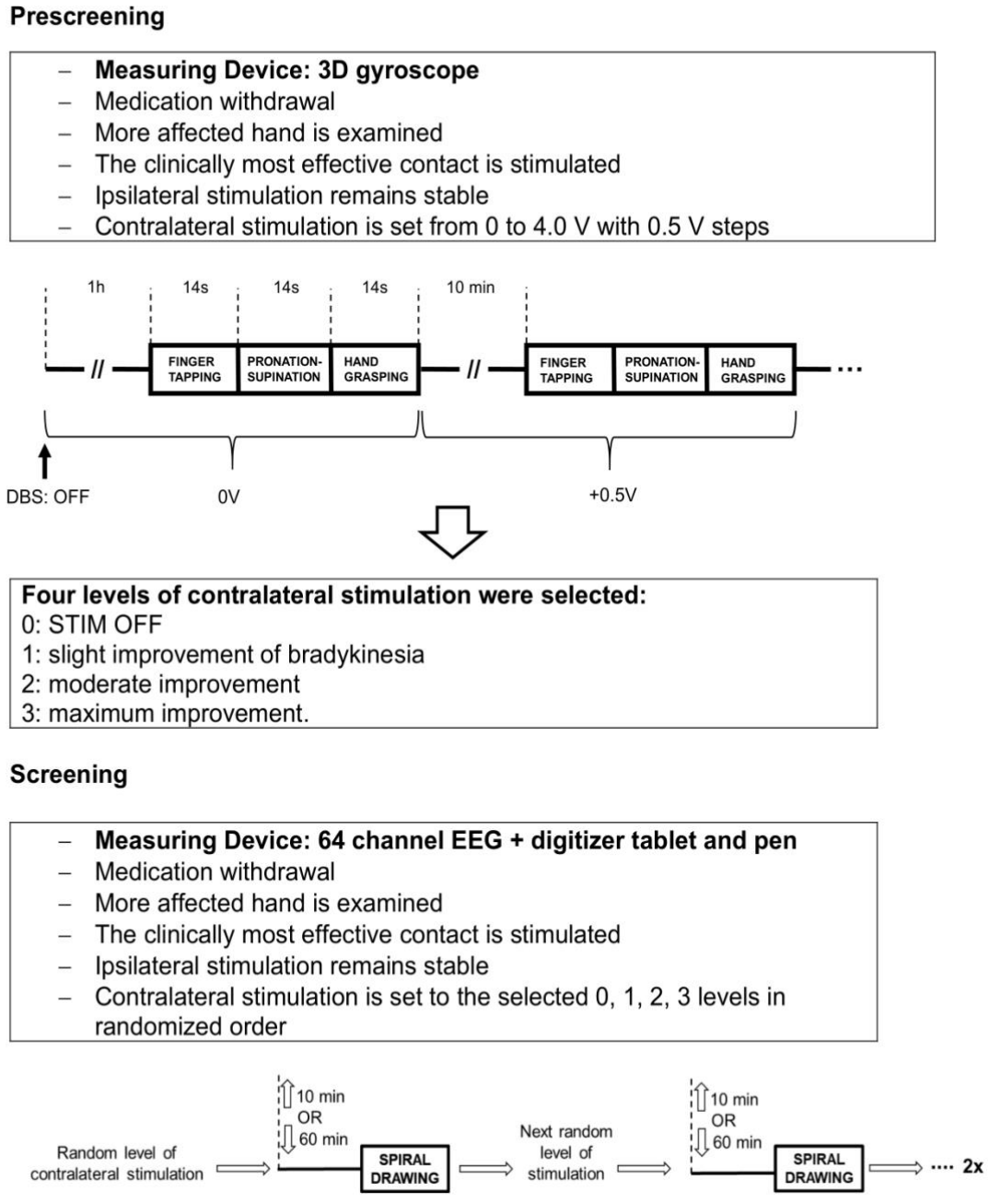

Figure 2. Study protocol (112)

3.5. Primary measurement, spiral acquisition, and analyses

The day following the prescreening, we performed the primary measurement after a 12-h medication withdrawal. Patients were comfortably seated in front of a table and asked

to draw Archimedean spirals with the most affected hand five times with a template (traced) and five times voluntarily (without a template, self-paced) on the four previously selected stimulation levels. We used a wireless inking pen and a digitizer tablet placed on the table [Wacom Bamboo Fun Pen and Touch Small Tablet CTH 461, Wacom Technology Corporation, Vancouver, WA, with a resolution of 2540 lpi (1000 points/cm), a sample frequency of 100 Hz, a pen active area of 14.72 × 9.20 cm, and a pressure sensitivity of 1024 levels]. First, subjects were asked to trace a template Archimedean spiral (spacing = 1.5 cm, maximal radius covered by the active zone of the tablet = 5.0 cm, three loops) printed on a sheet of paper (DIN A4 format = 24.0 × 29.7 cm) and attached to the surface of the tablet. Second, patients were asked to freely draw a spiral on the tablet without spatial constraints (i.e., without a template). At the beginning of every session, the patients were instructed to sit with their shoulders parallel to the front edge of the tablet and to draw at their own speed, starting from the center and ending at the border of the active zone without lifting the pen in between. In the case of traced drawing, the border of the active zone was marked on the template; patients were also asked not to cross the lines of the printed spiral. Before data collection, participants were allowed to practice. Spirals were drawn clockwise (right hand) or counterclockwise (left hand) depending on the more affected hand. Sessions of voluntary spiral drawing followed the traced drawing in every patient. The four selected stimulation levels were applied in counterbalanced order. The drawings were checked right after the sessions, and the patients drew additional spirals when necessary to reach a total of 5 appropriate spirals for a given condition and stimulation setting. The digital tablet was connected to a computer via a standard USB cable.

Kinematic data points were recorded using the Neuroglyphics software (http://www.neuroglyphics.org) (113), a Microsoft-based Windows application developed for kinematic information recording and analysis. The movement onset and end were visually checked and marked offline. Based on the instantaneous X and Y coordinates, the software determined the first-, second-, and third-order derivatives of position (Figure 3). To accurately characterize the motion of the pen along the circular path, we extracted the tangential velocity calculated for every data point. For this, the software estimated the rate of change of the angular displacement, which was then multiplied by the instantaneous radius of the spiral. Tangential velocity is the linear

velocity of an object moving along a circular path, measured at an arbitrary instant. Hereupon, we calculated the average and peak values of tangential velocity along with the sample entropy of tangential velocity for every spiral drawing. Sample entropy measured the average uncertainty of a random variable and was estimated with the MATLAB software (The MathWorks, version R2018b, Natick, MA, USA) function SampEn (114). In the case of time series, the sample entropy can be defined as the negative of the natural logarithm of the probability that two similar data sets with the length m remain similar if one more data point is added to each of them. We set the length of sequences to $m = 2$. The boundary of similarity above, in which two data sets are considered different, is represented by r. It ranges from 0 to 1; in our case, r was set to 20% of the time-series standard deviation (SD). The higher the entropy value, the greater the irregularity of a time series. Parameters of five spirals at each stimulation level were averaged for further statistical analysis.

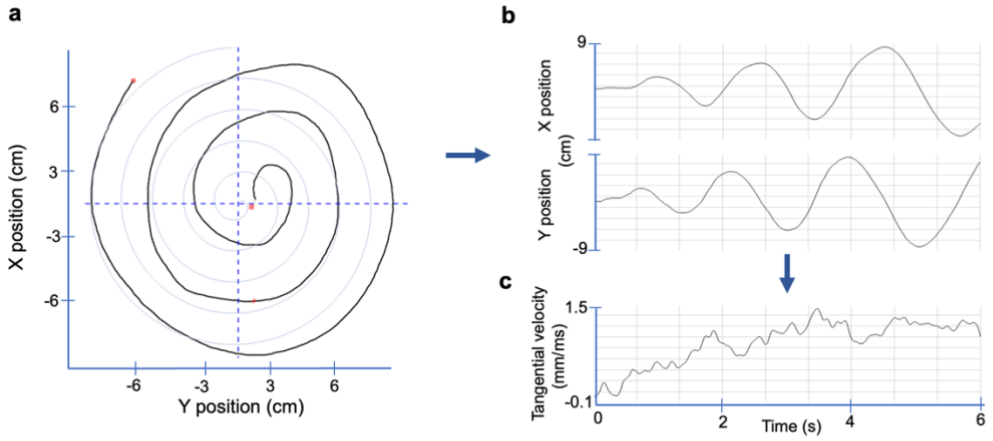

Figure 3. Digitized spiral processing pipeline (a) Spiral acquisition and **(b)** offline signal processing. For each spiral drawing, **(c)** the average tangential velocity was calculated (112)

3.6. EEG acquisition and preprocessing

We recorded an EEG file while patients drew five spirals voluntarily and another file while they drew traced spirals under one stimulation condition. These two files were recorded separately for each stimulation condition (4 × 2 files per patient). The following analysis steps were run separately on these files. Signals were recorded using a 64-channel EEG system (BrainVision Recorder, Brain Products Co., Munich, Germany), sampled at 2500 Hz (Figure 4).

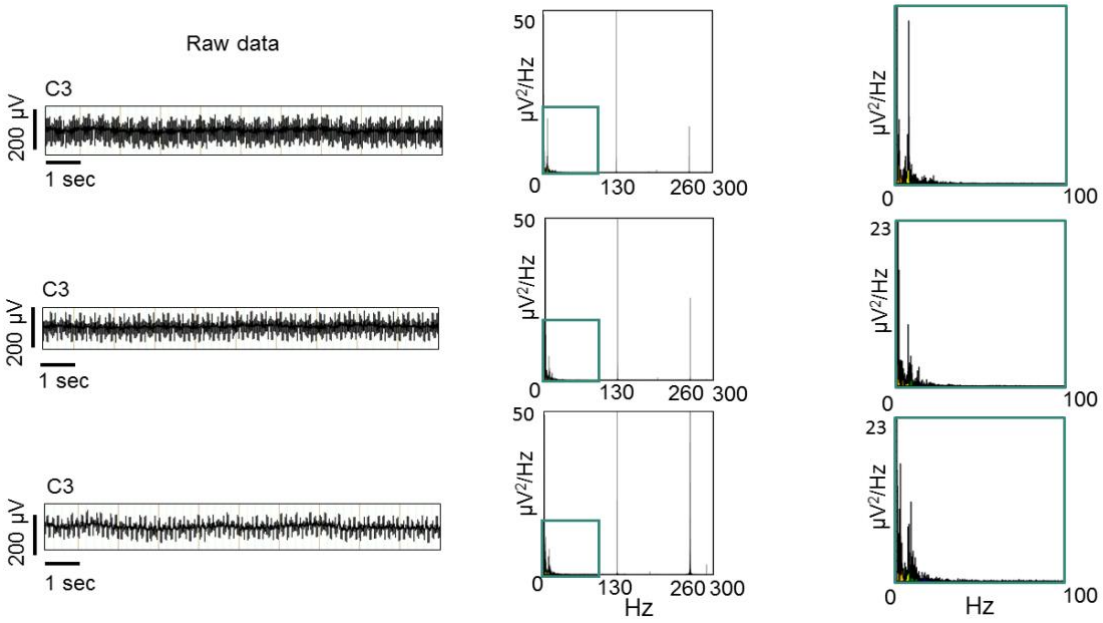

Figure 4. EEG recording under maximum stimulation amplitude Representative EEG time series and corresponding power spectral densities of non-saturated C3 (central 3) channels from three patients were recorded during the maximum stimulation level of the left subthalamic nucleus (112)

The initial preprocessing steps were performed by researchers who were blinded to the stimulation conditions. Preprocessing was carried out using MATLAB and BrainVision Analyzer (Brain Products Co., Munich, Germany). In the first step, the data were re-referenced to a common grand-average reference across all EEG channels. Then, data were filtered with a fourth-order Butterworth filter: 0.5 Hz high-pass, 300 Hz low-pass, followed by notch filters at 50, 100, and 150 Hz. In the next step, data were subjected to independent component analyses (ICA and inverse ICA) to remove components related

to DBS (Figure 5), muscle, eye blink, eye movement, and line noise artifacts. On average, 6 of 64 components [6.19 ± 1.17 (mean ± SD)] were rejected (DBS artifact: 2 ± 2.21; eye artifact: 1 ± 1.05; line noise: 2 ± 0.74; muscle artifacts: 1 ± 0.31). Residual muscle artifacts were visually inspected, removed, and interpolated with the cubic interpolation method. In the last step, EEG data recorded during the drawing of five spirals at a given stimulation level were concatenated for further statistical analysis.

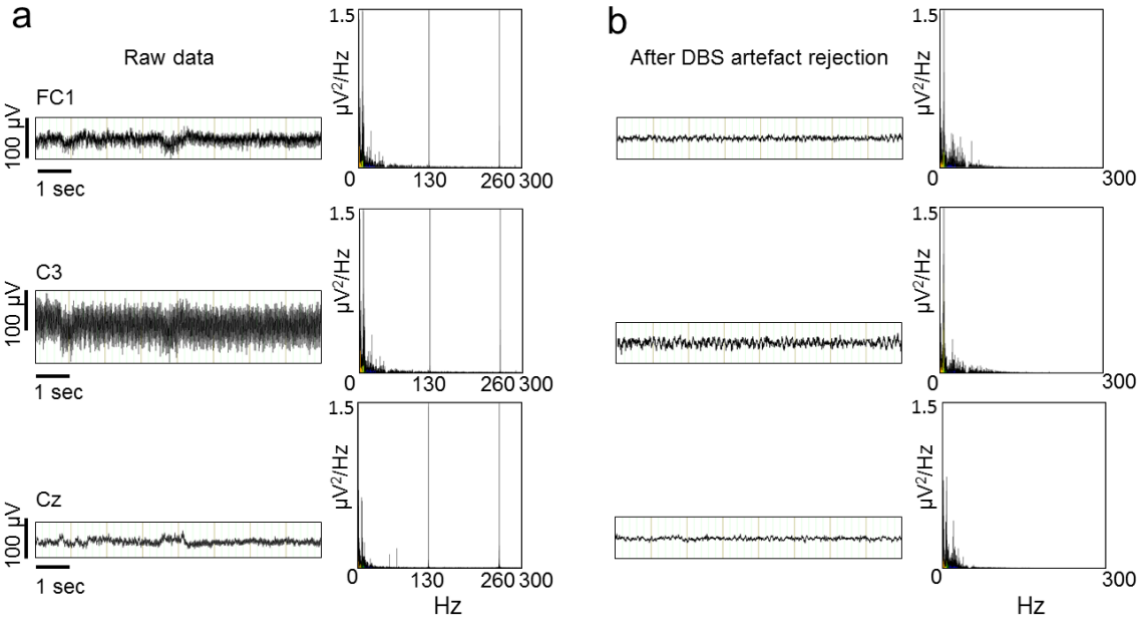

Figure 5. EEG preprocessing pipeline (**a**) Representative notch-filtered time-series data from three EEG channels (frontocentral channel 1: FC1; central channel 3: C3; midline central channel: Cz) of a patient receiving left STN-DBS during spiral drawing and its corresponding power spectral density (PSD) showing the power artifact created by the stimulation frequency (130 Hz) and its harmonic frequency (260 Hz). (**b**) Cleaned time series after independent component analysis, DBS artifact rejection, and corresponding PSD (112)

3.7. EEG source reconstruction

To reconstruct scalp potentials from a set of neural current sources, we modeled the propagation of neural electrical currents that produce differences in electrical potentials measured by surface sensors (Figure 6). For this, we used the Brainstorm software (115)

and applied the forward solution with a Finite Element Method (FEM), which estimated a lead-field matrix (LFM) for the brain (116). The LFM maps the contribution of a given source activation to potentials at different sensor locations. We proceeded with the following steps for every T1 MRI scan and individual electrode location. (A) A non-linear normalization of the MRIs was performed according to the MNI (Montreal Neurological Institute) stereotaxic coordinates implemented in the Statistical Parametric Mapping (SPM12) plugin (117). (B) The CAT12 plugin was used for cortical surface segmentation. (C) The segmentation of the head volume in different tissues (white matter: WM, gray matter: GM, cerebrospinal fluid: CSF, skull, and scalp), represented as high-quality tetrahedral 3D meshes, was achieved with SimNIBS (118). (D) The head model was generated with DUNEuro based on the individual T1 images and the tetrahedral mesh using a continuous Galerkin solver type and Venant source model with a 5 mm grid resolution (119). For the FEM layers, we assumed isotropic conductivity and used standard values for each: 0.14 S/m (siemens per metre) for WM, 0.33 S/m for GM, 1.79 S/m for CSF, 0.008 S/m for the skull, and 0.43 S/m for the scalp. (E) Source computation for each recording and individual electrode location was performed with a linearly constrained minimum variance (LCMV) beamforming method. LCMV is a spatial filtering procedure that monitors neural activity specified in the head model and estimates their relative contributions to sensor data by passing the electrical activity from a given location while attenuating contributions from other locations. It is applied to the whole brain, allowing a map of neural power to be created. The LCMV spatial filtering for the inverse solution was performed as described by Van Veen et al. (120). For LCMV beamformers, data noise and signal covariance matrices were estimated first, directly from the recordings. The estimated neural activity was used in further processing. We extracted the relevant motor areas involved in the spiral drawing using the Human Motor Area Template atlas (121) for the M1, SMA, pre-SMA, dorsal PMC, ventral PMC, dorsolateral prefrontal cortex (DLPFC), visual cortex (VC), and the Atlas of the basal ganglia (122) for the STN.

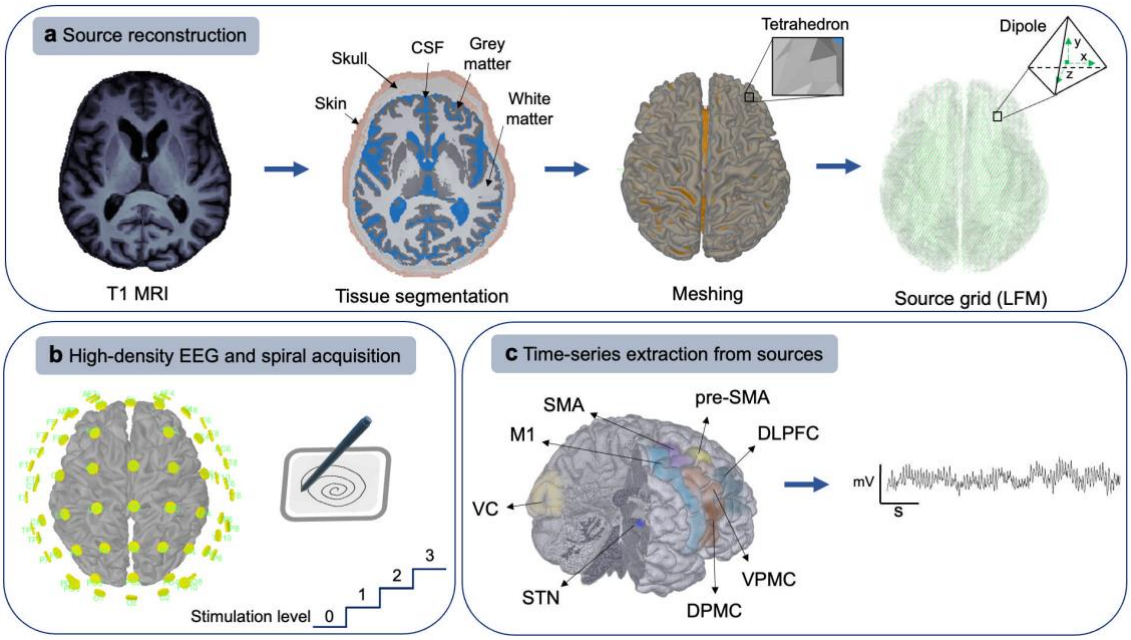

Figure 6. Signal processing pipeline (**a**) Based on individual T1 MRI sequences, we reconstructed a lead-field matrix using the Finite Element Method. (**b**) High-density EEG acquisition during traced and self-paced spiral drawing at four different stimulation levels. (**c**) Estimation of coherent neural activity and source extraction from the selected regions (112)

3.8. EEG analyses

3.8.1. Power spectral density analysis

To perform spectral analysis, a Welch's periodogram (50% overlap between 1-s Hamming windowed segments) was applied to the artifact-free electroencephalographic signal. The length of the concatenated epochs was 64.7 ± 23.7 s. The power was computed for 4 different frequency bands: low beta (13–20 Hz), high beta (21–30 Hz) (123), low gamma (31–60 Hz), and high gamma (61–100 Hz) (124) bands at each of the eight regions separately. We calculated the power values for both contralateral and ipsilateral to the drawing of self-paced and traced spirals.

3.8.2. Generalized partial directed coherence analysis

We used the generalized partial directed coherence (gPDC) method (125) to determine directed connectivity between M1, SMA, DPMC, VPMC, and STN. The gPDC method quantifies the frequency-domain direct causal relation using the transformed multivariate autoregressive coefficients A(f). This method considers the variance (σ) of the original signal and introduces a normalization factor in the denominator. This results in a normalized quantity (π) describing the ratio of outflow from the region j to i in relation to all outflows from region j:

$$\left|\pi_{ij}(f)\right| = \frac{\frac{1}{\sigma_i}\left|\bar{A}_{ij}(f)\right|}{\sqrt{\sum_{k=1}\frac{1}{\sigma_k^2}\left|\bar{A}_{k,j}(f)\right|^2}}$$

We estimated the gPDC for the low beta, high beta, low gamma, and high gamma frequency ranges.

3.9. Prediction analysis

In this work, we applied support vector machine (SVM) models with a Gaussian kernel (126) on the source power features derived from eight regions of interest, namely (M1, SMA, pre-SMA, DPMC, VPMC, STN, DLPFC, VC), to predict the slope of the spiral velocity computed from the spirals drawn at four different stimulation amplitudes. In this work, SVM models were trained using the Statistics and Machine Learning Toolbox in MATLAB (R2019a; MathWorks, Natick, Massachusetts, United States of America) with default kernel coefficients and regularization parameters. The complete description of default fitting parameters can be found in MATLAB (MathWorks. Fit a support vector machine regression model. https://de.mathworks.com/help/releases/R2019a/stats/fitrsvm.html, 2019) (127). In this study, SVM models were trained on the source power of traced spirals (eight slope values

from eight ROIs) and self-paced spiral source power values. To determine the impact and the contribution of each source power feature from each region on the predicted output of SVM, we used the Shapley value-based explanation known as Kernel SHapley Additive exPlanations (SHAP) (128).

3.10. Statistical analyses

Data analysis was performed using the statistical software TIBCO Statistica version 14.0.1. The normality of the data was assessed using the Kolmogorov-Smirnov test. Descriptive statistics were presented according to the data distribution. To compare the rates of change in tangential velocity and sample entropy across the different stimulation levels, we extracted the slopes for each parameter. We compared them using the paired t-test and the Wilcoxon matched-pairs signed rank test. We compared the average tangential velocity and the entropy of tangential velocity separately at the four stimulation levels in each task. We also analyzed beta and gamma power spectral densities and connectivity strength at the four stimulation levels. Repeated measures analysis of variance (ANOVA) was used, with the post hoc Tukey test, to detect differences in spiral parameters, power spectra, and connectivity strength across stimulation levels. For the graphomotor tasks, the within-group effects were TASK (self-paced and traced spiral drawing) and STIMULATION LEVEL (0–3). In the case of power spectral density analysis, we used the following within-group effects: TASK (self-paced and traced spiral drawing), BAND (low beta, high beta, low gamma, and high gamma), REGION (M1, DLPFC, VPMC, DPMC, pre-SMA, SMA, VC, STN), HEMISPHERE (contralateral and ipsilateral to the task), STIMULATION LEVEL (0–3). For connectivity analysis, we analyzed the TESTED SIDE (left and right) as a between-group effect, the within-group effects were as follows: TASK (self-paced and traced spiral drawing), BAND (low beta, high beta, low gamma, and high gamma), PAIR OF REGIONS between M1, SMA, VPMC, DPMC, and STN, STIMULATION LEVEL (0–3). The level of significance was set to $p < 0.05$.

4. Results

4.1. Clinical characteristics of the patients

Table 1 presents demographic data, disease-related information, and stimulation parameters. The study involved 24 male and 14 female patients, with a mean age of 65.6 ± 7.38 years. Mini-Mental State Examination (MMSE) scores measured at the time of spiral acquisition did not differ from preoperative MMSE scores (normal distribution, paired t-test, $p > 0.05$), as did Addenbrooke's Cognitive Examination scores (normal distribution, paired t-test, $p > 0.05$). Figure 7 displays the position of stimulating contacts within the sensorimotor region of the STN for all patients.

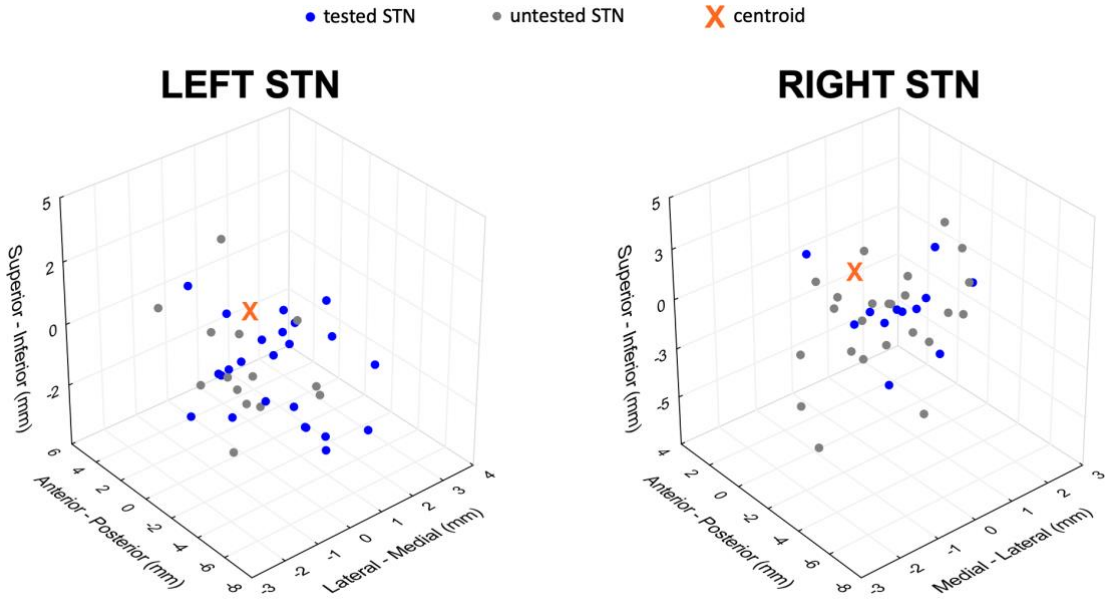

Figure 7. Active contact locations relative to the center point of the dorsolateral STN
The active contact locations are presented in the MNI space; the x-axis represents the medial-lateral, the y-axis anterior-posterior, and the z-axis superior-inferior plane. Tested contact locations in each STN contralateral to the movement are presented with blue dots. Gray dots depict contact locations of untested STN (ipsilateral to the movement) with stable stimulation. The center point of the dorsolateral STN is the point of reference, represented by an orange cross (112)

The mean distances (±SD) of the tested active contact from the center of the dorsolateral STN were: X: 1.04 ± 0.66 mm; Y: 2.46 ± 1.33 mm; Z: 1.25 ± 1.1 mm; 3D distance:

0.77 ± 0.76 mm. The patients performed self-paced and traced spiral drawing at four different stimulation levels in randomized order. Subsequently, the intensity (average $\pm$ SD) of the various stimulation levels was at level 0: 0 mA, at level 1: 1.25 ± 0.58 mA, at level 2: 2.32 ± 0.73 mA, and at level 3: 2.99 ± 0.84 mA.

Table 1. Demographics and clinical data of the recruited patients (112)

Mean age (SD)		65.6 (7.38) years
Sex		14 females, 24 males
Disease duration		13.2 (6.67) years
Elapsed time after operation		2.7 (2.20) years
Left STN stimulation	Amplitude	2.3 (0.59) mA
	Pulse width	59.9 (6.06) μs
	Frequency	134.8 (7.36) Hz
Right STN stimulation	Amplitude	2.3 (0.83) mA
	Pulse width	60.7 (7.78) μs
	Frequency	135.2 (7.4) Hz
Tested STN		24 left, 14 right
Preoperative UDPRS III.	MED OFF	23.1 (18.46) points
	MED ON	8.3 (9.03) points
UPDRS III. at the time of the study	STIM ON-MED OFF	10.7 (12.14) points
	STIM ON-MED ON	5.2 (6.47) points
Hoehn-Yahr stage	Preoperative	1.7 (0.83)
	At the study	1.3 (0.84)
Levodopa equivalent dose	Preoperative	745.3 (540.38) mg
	At the study	407.4 (281.07) mg
Mini-Mental State Examination scores	Preoperative (38/38 patients)	28.34 (1.26)
	At the study (38/38 patients)	28.32 (0.96)
Addenbrooke's Cognitive Examination scores	Preoperative (23/38 patients)	89.4 (5.35)
	At the study (35/38 patients)	87.4 (5.79)

4.2. Spiral drawing analysis

The average time needed to draw a single spiral was 14.3 ± 6.42 s, while the average time required to draw 5 spirals was 64.7 ± 23.71 s. The average tangential velocity was higher in the self-paced than in the traced drawings (repeated measures ANOVA; TASK factor: $F_{1,37} = 33.40$, $p < 0.0001$). It increased gradually with increasing stimulation intensity during both the self-paced and traced drawing tasks (STIMULATION LEVEL factor: $F_{3,111} = 27.43$, $p < 0.001$; Figure 8a). There was a significant difference in the slope of increase of the average tangential velocity, being higher in the case of self-paced spirals than traced spirals (non-normal distribution, Wilcoxon matched-pairs signed rank test, $p = 0.0035$). The velocity entropy was lower in the self-paced than in the traced spiral drawing (TASK factor: $F_{1,37} = 14.95$, $p < 0.0001$). In addition, the entropy of velocity in both tasks diminished when turning the stimulation on but did not change in parallel with increasing stimulation intensity (STIMULATION LEVEL FACTOR: $F_{3,111} = 12.74$, $p < 0.001$. Tukey significant post hoc comparisons: self-paced and traced drawing: $p_{0\text{-}1} < 0.05$, $p_{0\text{-}2} < 0.05$, $p_{0\text{-}3} < 0.05$; Figure 8b). The rate of decrease in the entropy of velocity did not differ between the two types of drawing (normal distribution, paired t-test, $p > 0.05$; Figure 8b).

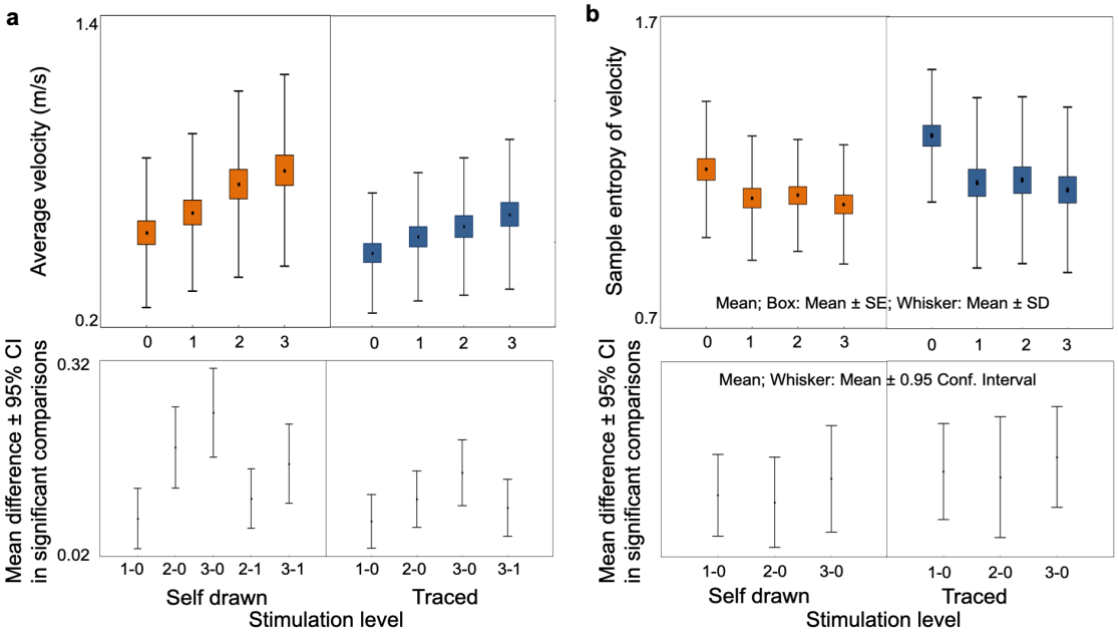

Figure 8. Average velocity and entropy of velocity of spiral drawing in the four levels of stimulation (**a**) Average tangential velocity increased in both self-paced and traced

spiral drawing tasks. (**b**) Entropy of velocity decreased when stimulation was switched on, but did not increase further with increasing intensity in each task. Repeated measures ANOVA revealed a significant main effect of stimulation level. Significant post hoc comparisons are presented in the bottom row ($p < 0.05$) (112)

4.3. Power spectral density analysis in the beta and gamma bands

During both self-paced and traced spiral drawings, the power spectral analysis of each frequency band revealed significant changes when modifying the DBS setting contralateral to the movement (ipsilateral to the stimulation) in the cortical areas (M1, DPMC, VPMC, SMA, pre-SMA, DLPMC) and the STN; LOC × BAND × SUBBAND × HEMISPHERE × STIM LEVEL within effect interactions: self-paced task: $F_{24,432} = 1.8$, $p = 0.012$; traced task: $F_{24,456} = 2.4$, $p = 0.0002$; post hoc Tukey comparisons are shown in the top rows of Figure 9, Figure 10, Figure 11, Figure 12, Figure 13, Figure 14, Figure 15. As the stimulation intensity increased, we observed a gradual decrease in both low beta and high beta power, accompanied by a gradual increase in low gamma and high gamma power during the graphomotor tasks contralateral to the movement (ipsilateral to the stimulation). Power values in the four frequency bands in the cortical areas and the STN ipsilateral to the movement (contralateral to the stimulation) were not influenced by changes in DBS intensity (post hoc Tukey comparisons are shown in the bottom rows of Figure 9–15). We chose the visual cortex as a reference because it is not involved in motor actions; neither beta nor gamma band activity changed with the adjusted stimulation intensities (Figure16).

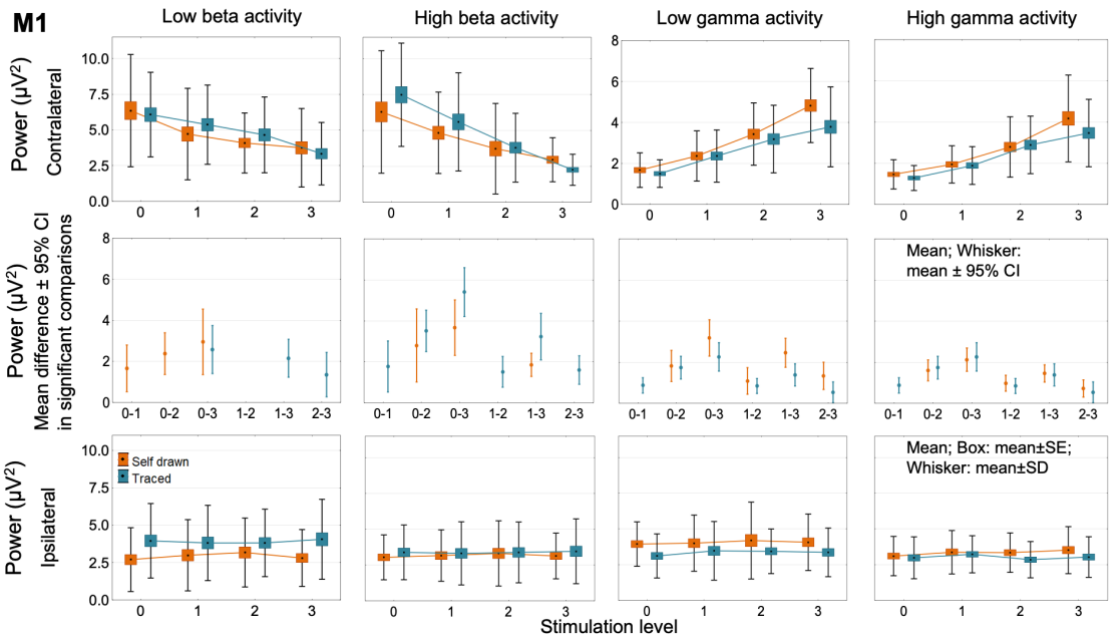

Figure 9. Absolute beta and gamma power changes in the primary motor cortex (M1) In the primary motor cortex, subthalamic stimulation decreased absolute low and high beta band power stepwise in the tested hemisphere (contralateral to the movement). At the same time, both low and high gamma activity increased with increasing stimulation intensity. Power differences in significant post hoc comparisons of stimulation level effect are presented in the middle row. Bottom row: in the untested hemisphere (ipsilateral to the movement), beta and gamma power remained unchanged as stimulation intensity increased (112)

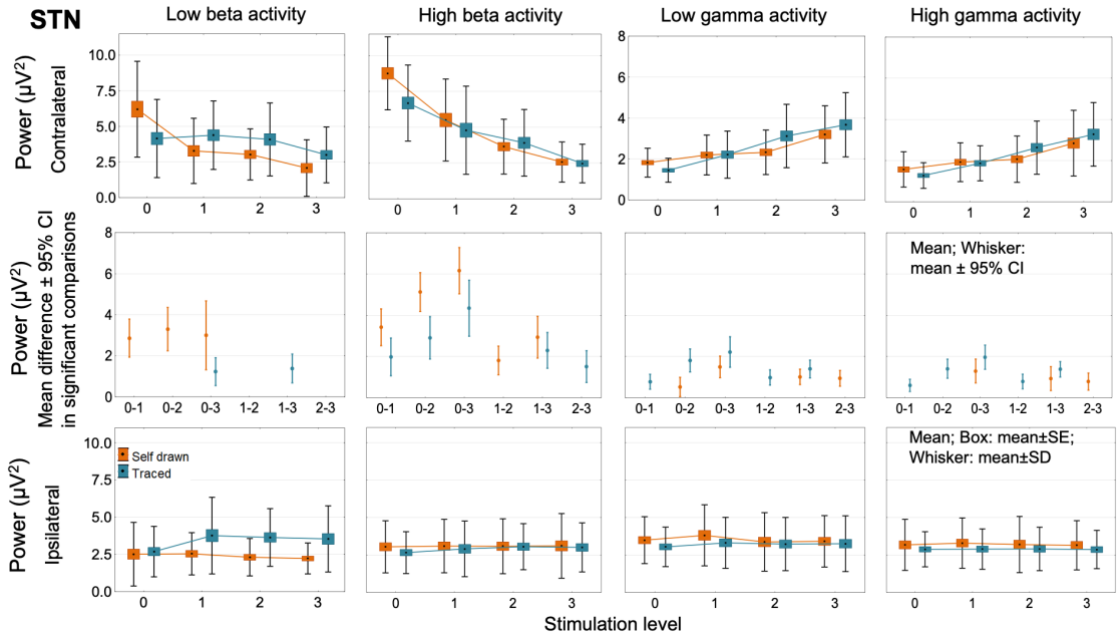

Figure 10. Absolute beta and gamma power changes in the subthalamic nucleus (STN) Stimulation-induced power changes in the low beta, high beta, low gamma, and high gamma bands in the STN are similar to the changes observed in the primary motor cortex (Figure 9) (112)

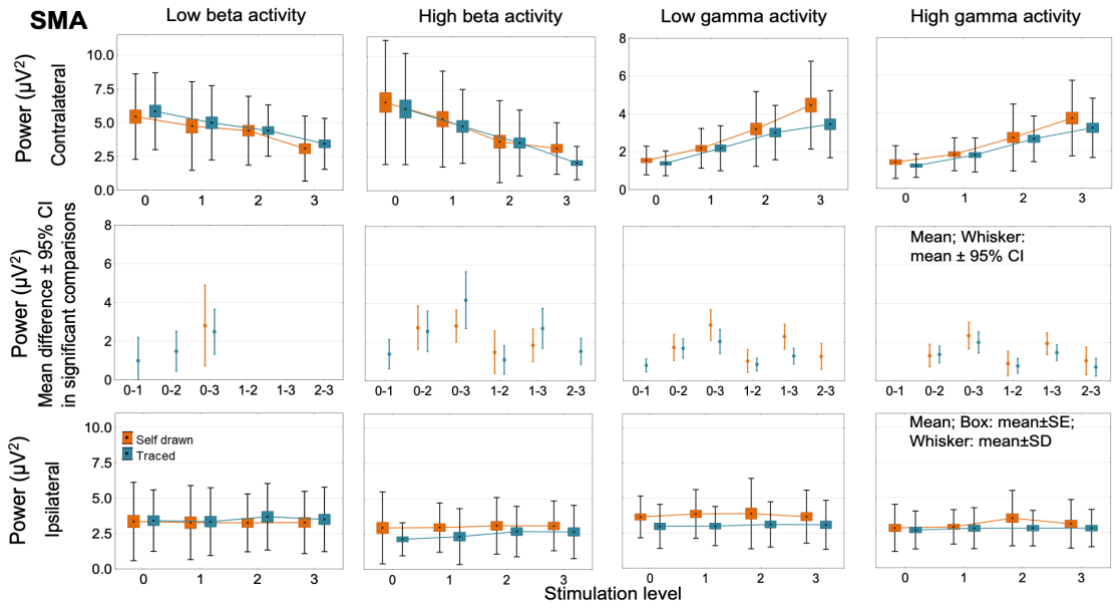

Figure 11. Absolute beta and gamma power in the supplementary motor area (SMA) Power value changes in the tested hemisphere induced by stimulation in the low beta, high beta, low gamma, and high gamma bands in SMA are similar to the changes in the primary motor cortex. Power differences in significant post hoc comparisons of stimulation level effect are presented in the middle row. Bottom row: beta and gamma

power remained unchanged with rising stimulation intensity in the not-tested hemisphere (ipsilateral to the movement) (112)

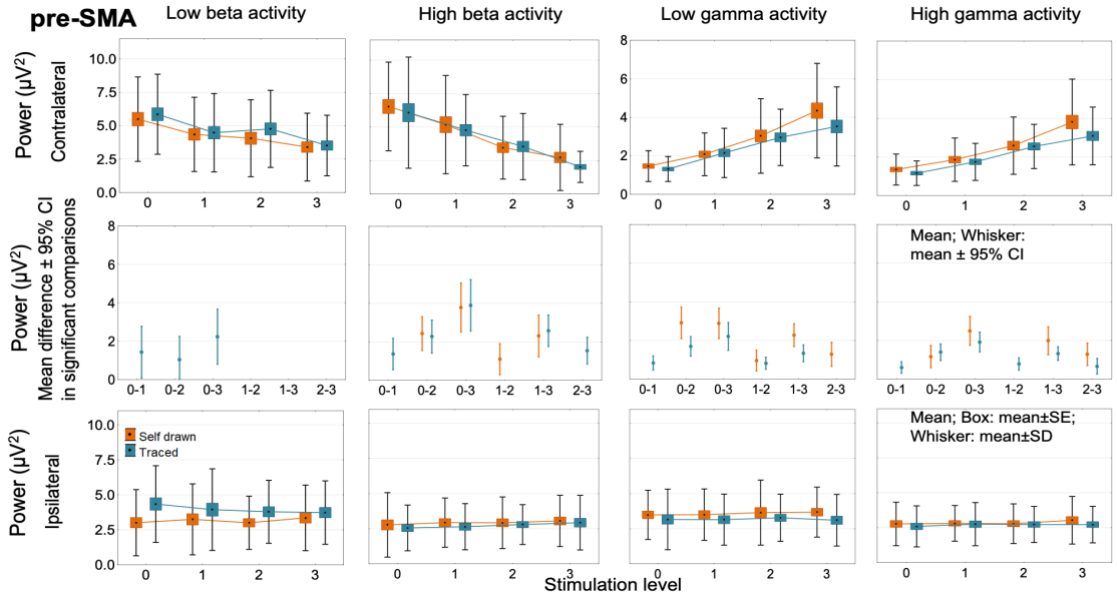

Figure 12. Absolute beta and gamma power in the pre-supplementary motor area (pre-SMA) Significant post hoc comparisons assessing the effect of stimulation intensity on power are shown in the middle row. In contrast, the bottom row shows that beta and gamma power in the non-tested hemisphere remained unchanged (112)

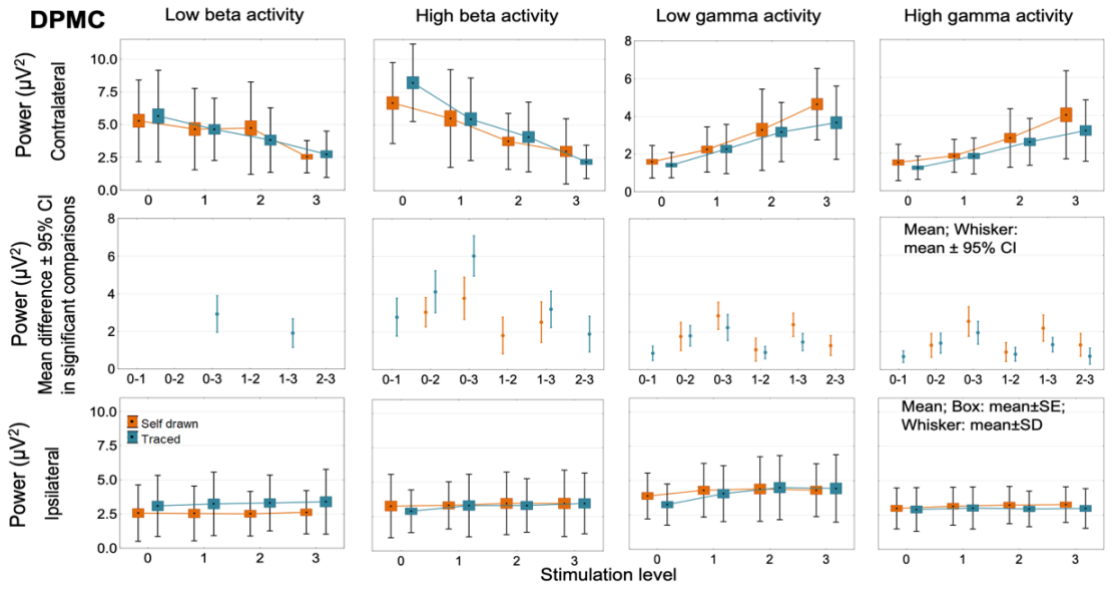

Figure 13. Absolute beta and gamma power in the dorsal premotor cortex (DPMC) Stimulation-induced changes were similar to those observed in the primary motor cortex (112)

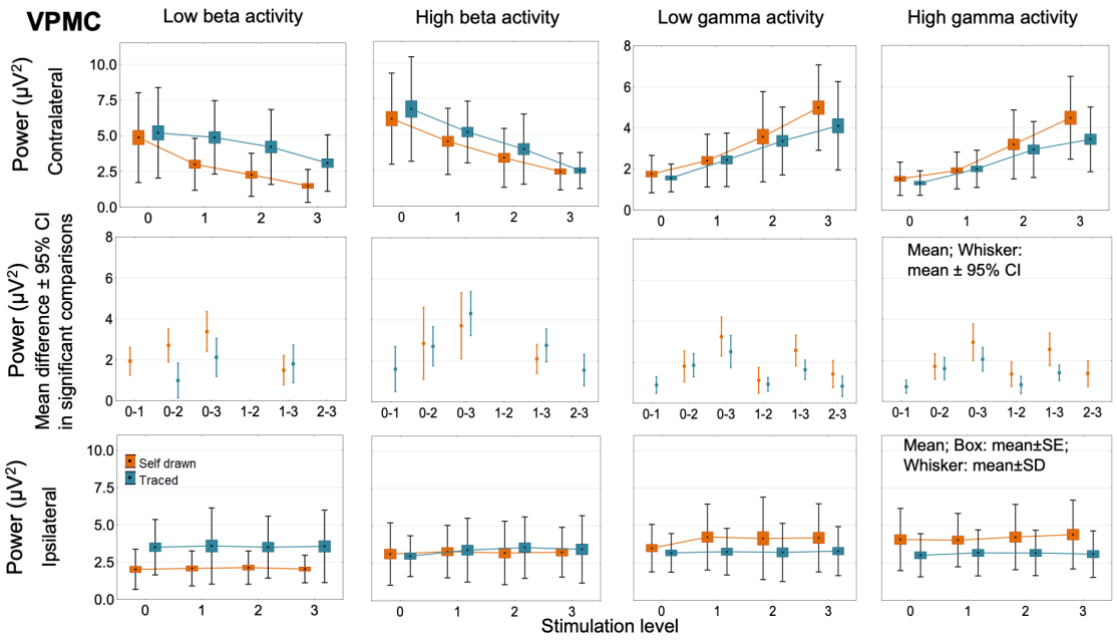

Figure 14. Absolute beta and gamma power in the ventral premotor cortex (VPMC) Stimulation-induced changes were similar to those observed in the primary motor cortex (112)

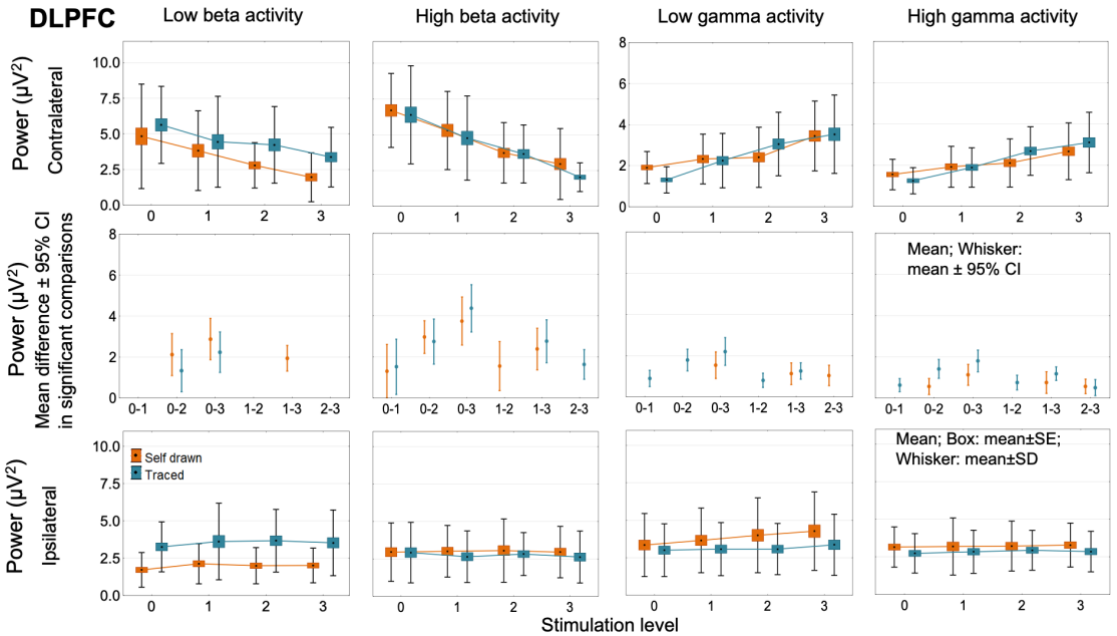

Figure 15. Absolute beta and gamma power in the dorsolateral prefrontal cortex (DLPFC) Stimulation-induced changes were similar to those observed in the primary motor cortex (112)

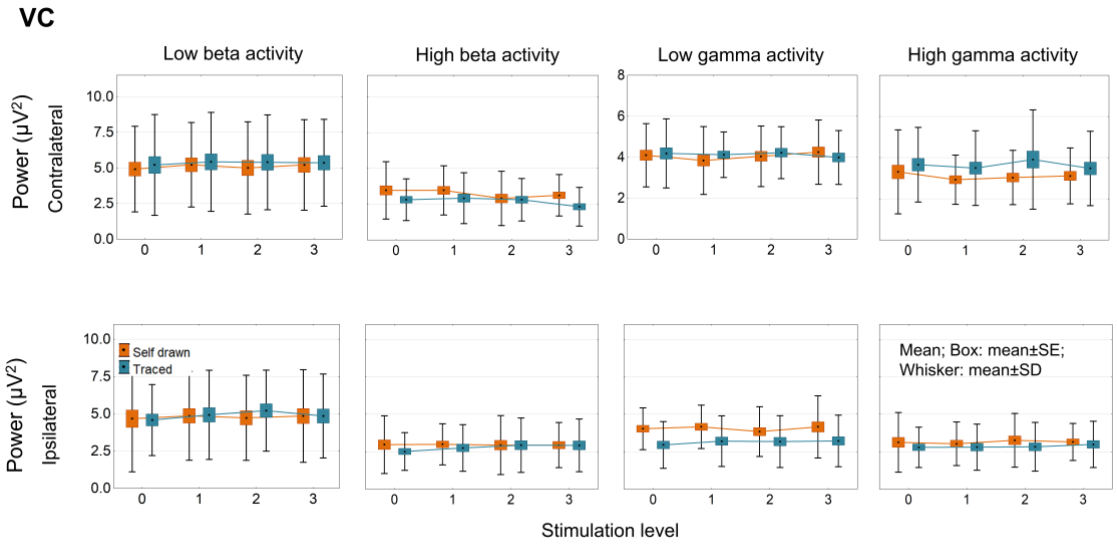

Figure 16. Absolute beta and gamma power in the visual cortex (VC) Subthalamic stimulation did not affect absolute power in any of the analyzed frequency bands in the visual cortex, used as a reference region relative to the motor areas (112)

4.4. Prediction analysis

We examined whether we could predict the stimulation-induced improvement (slope of data set at the 0–3 stimulation levels) in self-paced and traced spiral drawing speed from the stimulation-induced low, high beta, and gamma power changes (slope of data set at the 0–3 stimulation levels) of the cortical motor sources and the STN. The optimal model for both self-paced and traced spirals was trained on eight EEG spectral power features for each frequency band separately. The prediction accuracy of R-squared for self-paced was $R^2 = 0.63 \pm 0.1$, and for traced spirals: $R^2 = 0.71 \pm 0.03$. Based on the mean absolute SHAP values, we identified the most influential features affecting the SVM prediction of stimulation-induced change in self-paced spiral drawing speed. High beta power in the DLPFC, DPMC, and M1 emerged as key factors. High gamma power in the M1, SMA, and DLPFC, with SHAP values of 0.019, also significantly contributed to deviations from the average prediction of self-paced drawing speed slope across all instances (Table 2). The stimulation-induced power slopes of sources in the four frequency bands did not reliably predict the drawing speed slope of traced spirals (Table 3).

Table 2. Shapley Values for all regions of interest (ROIs) and analyzed frequency bands in self-paced spiral drawings Stimulation-induced changes in M1-related high beta and high gamma network activity predicted the parallel increase in drawing velocity. Significant contributions are displayed in bold (112)

ROI	M1	SMA	pre-SMA	DPMC	VPMC	STN	DLPFC	VC
Low Beta	0.0091	0.00905	0.00905	0.0089	0.0089	0.0091	0.00905	0.0089
High Beta	**0.0193**	0.0090	0.0090	**0.0192**	0.0090	0.0090	**0.02**	0.0090
Low Gamma	0.00905	0.0091	0.0089	0.0089	0.0089	0.0089	0.0088	0.0088
High Gamma	**0.019**	**0.019**	0.0085	0.0086	0.0086	0.0085	**0.019**	0.0085

Table 3. Shapley Values for all regions of interest (ROIs) and analyzed frequency bands in traced spiral drawings We could not detect any stimulation-induced network activity, which could predict the traced spiral drawing velocity changes (112)

ROI	M1	SMA	pre-SMA	DPMC	VPMC	STN	DLPFC	VC
Low Beta	0.0087	0.0086	0.0085	0.0089	0.0088	0.0093	0.0089	0.0088
High Beta	0.0088	0.0087	0.0086	0.0090	0.00905	0.0089	0.0089	0.0088
Low Gamma	0.00905	0.0090	0.00905	0.0089	0.0090	0.0090	0.0088	0.0091
High Gamma	0.0090	0.0088	0.0085	0.0087	0.0088	0.0086	0.0095	0.0088

4.5. Effective connectivity

We investigated how effective connectivity between sources is affected by stimulation intensity. For both self-paced and traced spiral drawings, the generalized partial directed coherence effective connectivity (EC) in the high beta band decreased with increasing stimulation intensity between the STN and the cortical areas, such as M1, SMA, VPMC, and DPMC contralateral to the movement, and the effect was present on both direction (STN to motor cortex: STIMULATION LEVEL factor: $F_{3,68} = 84.17$, $p < 0.0001$; motor cortex to STN: STIMULATION LEVEL factor: $F_{3,68} = 19.07$, $p < 0.0001$) (post hoc Tukey comparisons: Figure 17 and Figure 18). We compared the tested left hemispheres (24 patients) with the tested right hemispheres (14 patients), and there was no difference in the EC values (TESTED SIDE factor: $F_{1,22} = 0.34$, $p > 0.05$). At the same time, EC increased in the high gamma band between M1 and premotor cortical areas (SMA,

VPMC, and DPMC) in both directions (M1 to premotor cortical areas: STIMULATION LEVEL factor: $F_{3,68} = 49.93$, $p < 0.0001$; premotor cortical areas to M1: STIMULATION LEVEL factor: $F_{3,68} = 62.88$, $p < 0.0001$), but not between STN and motor cortical areas ($p > 0.05$ in all post hoc Tukey test comparisons as shown in Figure 19 and Figure 20), or among the SMA, DPMC and VPMC ($p > 0.05$ in all post hoc Tukey test comparisons). In the analyzed regions, there was no stimulation-induced change in EC in the low beta and low gamma frequency bands ($p > 0.05$ in all comparisons). There was no significant difference in connectivity values measured during traced and self-paced drawings (TASK factor: $F_{1,15} = 0.029$, $p > 0.05$).

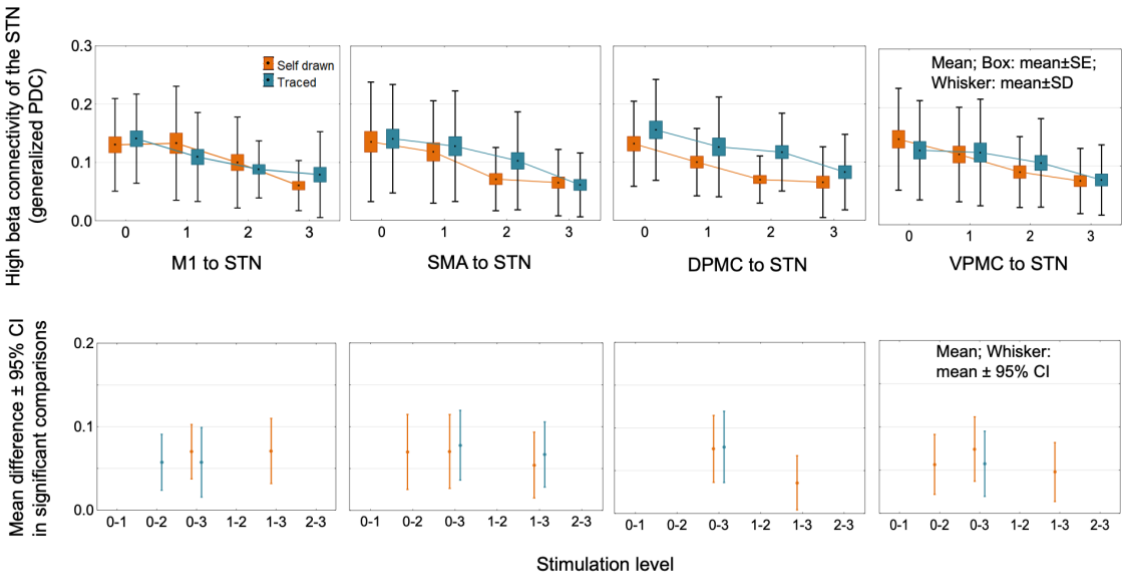

Figure 17. Stimulation effects on task-related hyperdirect high beta effective connectivity in PD patients: cortico-subthalamic direction Effective connectivity between the motor cortical areas and STN decreased in the high beta band with increasing stimulation intensity. Significant comparisons of stimulation level effects are presented in the bottom row. The figure visualizes the direction of coherence from motor cortical areas toward the subthalamic nucleus. However, this effect was bidirectional; the opposite direction of effective connectivity is shown in Figure 18 (112)

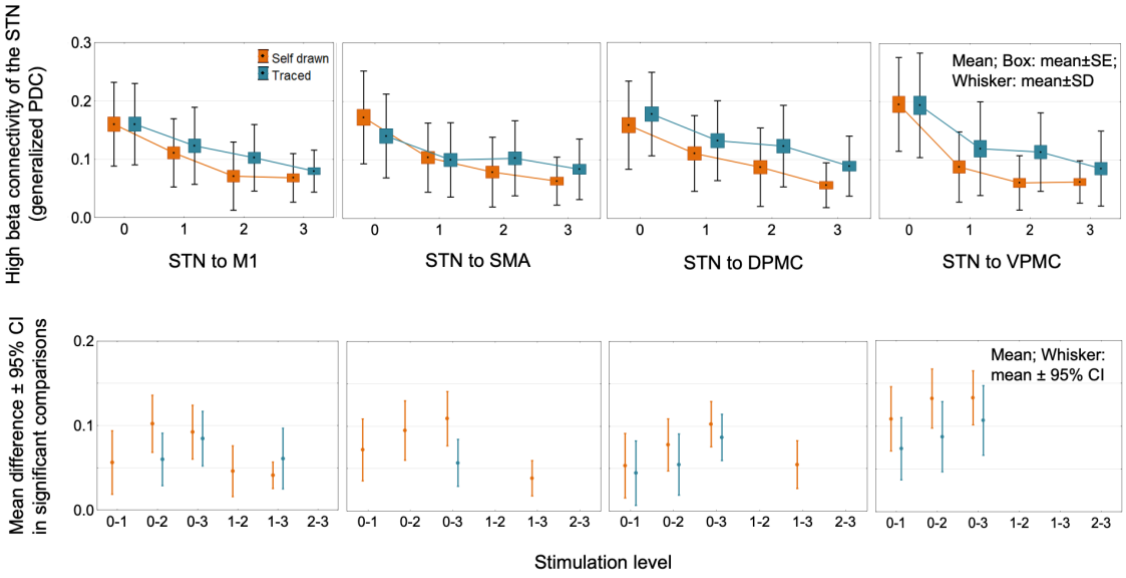

Figure 18. Stimulation effects on hyperdirect high beta connectivity: subthalamo-cortical direction Effective connectivity between the STN and motor cortical areas decreased in the high beta frequency band with increasing stimulation intensity in a bidirectional manner. Cortico-subthalamic connectivity changes are shown in Figure 17; here, we present the decrease in subthalamo-cortical effective connectivity. Significant post hoc comparisons of stimulation level effect are presented in the bottom row (112)

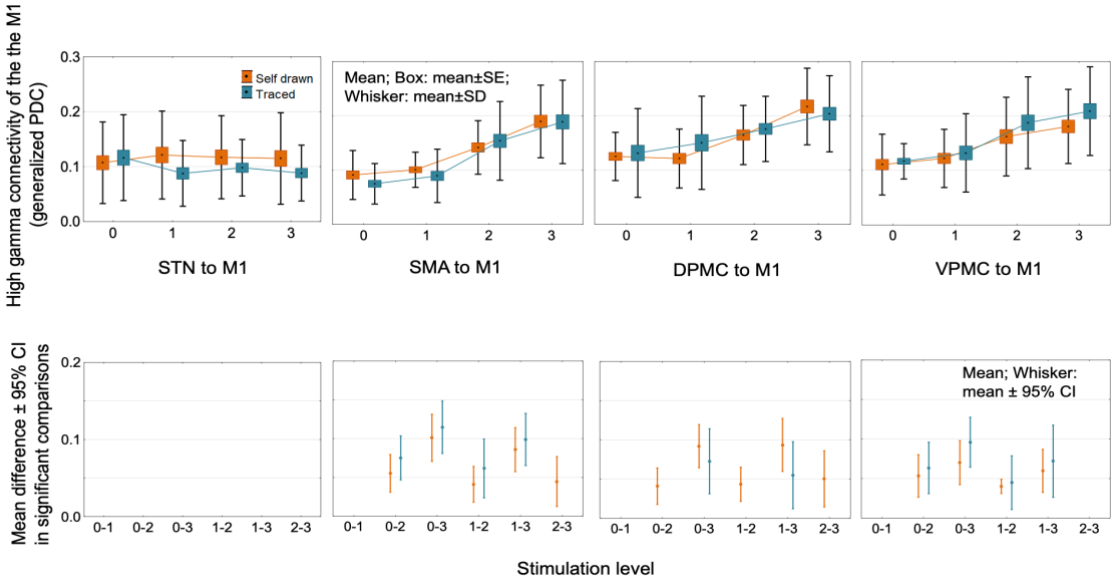

Figure 19. STN stimulation increases the high gamma effective connectivity between the premotor cortical areas and the M1 Ramping subthalamic stimulation increased

effective connectivity between premotor cortical areas and M1 in the high gamma frequency band; however, high gamma STN-M1 effective connectivity remained unaffected. Significant post hoc comparisons of the stimulation level effect are presented in the lower row. The effect was bidirectional; effective connectivity from the direction of M1 to other structures is presented in Figure 20 (112)

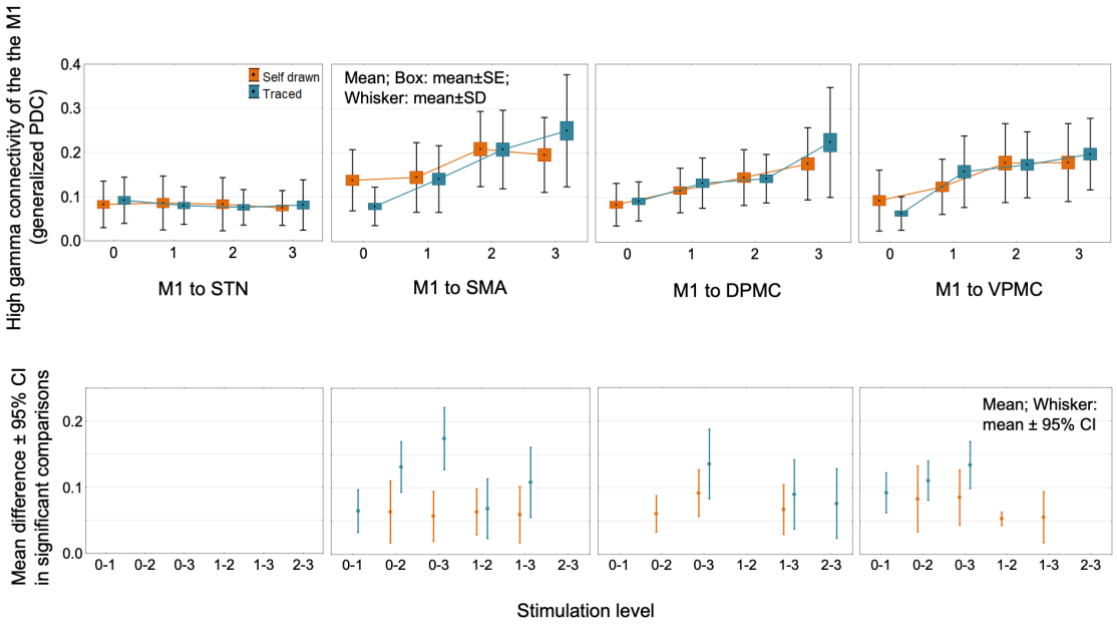

Figure 20. Stimulation effects on task-related cortico-cortical and cortico-subthalamic high gamma connectivity This figure shows the direction from M1 to the other structures. Effective connectivity from the STN to cortical structures is presented in Figure 19 (112)

5. Discussion

Our study explored the frequency-specific network effects of subthalamic nucleus stimulation during complex hand movements in patients with Parkinson's disease. First, we showed that STN DBS suppressed the synchronized high beta band oscillatory activity between the STN and motor cortical areas while facilitating the high gamma information flow between the motor cortical areas in a dose-dependent manner during traced and self-paced spiral drawing. Second, we showed that spiral drawing speed increased with increasing stimulation intensity. At the same time, low and high beta power and low and high gamma power gradually decreased and increased, respectively, throughout the cortico-subthalamic motor network during traced and self-paced spiral drawing. Third, we also showed that high beta and high gamma oscillations in networks, including M1, most accurately predict speed improvement in self-paced spiral drawing. What sets our study apart from previous findings in the literature is the assessment of STN stimulation-induced changes in the cortico-subthalamic connectivity profile during fine motor control under different stimulation intensities. Our study provides a dynamic characterization of cortico-subthalamic network modulation during fine motor control under gradually increasing stimulation intensities.

Using our source reconstruction model, we showed that subthalamic stimulation reduces connectivity between the STN and cortical regions, including the M1, SMA, DPMC, and VPMC, at the high beta (21–30 Hz) frequency range. STN-DBS did not influence cortico-subthalamic effective connectivity in the low beta, low gamma and high gamma frequency ranges.

The hyperdirect pathway plays a crucial role in the development of bradykinesia (129), and its subthalamic entry point represents the sweet spot for effective subthalamic deep brain stimulation in PD (130, 131). Our findings confirm that high beta synchrony along the hyperdirect pathway is a core pathological feature of bradykinesia and can be progressively attenuated by subthalamic stimulation.

An fMRI study has shown increased functional connectivity along the hyperdirect pathway, even in the early stages of PD (132), with a contralateral preponderance toward the more affected limb in the resting state (132). This phenomenon was decreased at rest

and increased during movement by STN-DBS, which was associated with better motor performance (133).

In STN local field potential (LFP) measurements combined with ECoG (24), EEG (134, 135), or MEG (17, 23, 25), it was previously shown that the high beta frequency connectivity is dominant along the hyperdirect pathway and decreases with STN stimulation (17, 25), which is consistent with our results. It was previously hypothesized that high beta activity in the hyperdirect pathway enhances subthalamic low beta oscillations, which correlate most with the severity of bradykinesia (17, 25).

Pathological high beta subthalamo-cortical coherence was also revealed in animal models of Parkinson's disease (136). It is debated whether the cortex (17, 24, 25, 134, 135) drives the STN or whether their connectivity is bidirectional (16, 137). It was suggested that the increased basal ganglia synchronization in the beta band might serve as a temporal reference frame for cortical gamma activity through the hyperdirect pathway (138), so the rhythmic activity in the STN results in fluctuating excitability in cortical neuronal assemblies (17).

An LFP study combined with MRI suggested that decreasing cortical thickness may play a role in the emergence of pathological high beta activity (139). According to our results, effective connectivity in the high beta band along the hyperdirect pathway diminishes gradually with increasing subthalamic stimulation in both directions. This supports the hypothesis that reducing pathological high beta coupling disrupts abnormal motor inhibition and facilitates more effective motor execution. However, it has also been described that the effective direction of coherent oscillatory activity in the basal ganglia is dynamic and depends on the brain state (140).

Earlier studies also found that STN activity at 60–90 Hz was coherent with activity in M1; directionality analysis showed that STN gamma activity at 60–90 Hz tended to drive gamma activity in M1 (86). In our study, we could not explore stimulation-reactive hyperdirect activity in the gamma bands. Previously, the hyperdirect pathway activity was shown to be lateralized. Functional MRI data of healthy subjects revealed that effective connectivity of the right hyperdirect and direct pathways could predict the best outcome of the stop-signal task (141). Furthermore, the lateralized activity of the STN was indicated by a resting state STN LFP study of 24 patients with Parkinson's disease, which revealed that phase-amplitude coupling between high beta (20–30 Hz) and high gamma

(70–100 Hz) oscillations is higher in the right STN than in the left STN irrespective to the asymmetry in pathophysiology, in the OFF-levodopa condition and reacts better to levodopa intake (142). In our study of 38 patients, we found that the subthalamo-cortical effective connectivity did not differ significantly between the more affected and the tested left and right hemispheres. Here, we assessed coherent activity between the two distinct regions, whereas the aforementioned study analyzed cross-frequency coupling (CFC) within the STN. Further studies are needed to unravel the role of CFC along the left and right hyperdirect pathways in patients treated with deep brain stimulation.

In our study, at the cortical level, subthalamic stimulation improved bidirectional effective connectivity between M1 and other motor cortical areas, such as the SMA, VPMC, and DPMC, parallel with the clinical improvement. The enhancement of cortical high gamma connectivity suggests improved intracortical communication, which may support movement initiation and execution. Still, this phenomenon was absent between the SMA and the premotor cortical areas.

Cortical dysfunction is also part of the compound network dysfunction related to bradykinesia in PD. Previously, in the resting state, pre-SMA showed deficient connectivity exposed by fMRI with surrounding cortical areas, including the ipsilateral premotor cortex, insula, and parietal cortex, and increased connectivity between pre-SMA and M1 (143). Earlier studies have scrutinized the lower gamma band connectivity at the cortical network level. A previous EEG study found an increased widespread cortical low gamma (30–45 Hz) synchrony in de novo PD patients (144), and the authors argued that it might be a transient compensatory mechanism of preserved cortical neurons and represents a motor capacity reactive to levodopa (86) and STN stimulation (145). EEG studies showed that augmented cortical gamma (35–50 Hz) connectivity in central cortical areas promotes movement initiation and execution (144). Globus pallidus internus and subthalamic nucleus DBS increased resting state synchrony in the 26 to 50 Hz frequency band between the prefrontal, motor, middle/inferior temporal, and occipitoparietal cortices in a MEG study (146).

It is unclear how the high gamma band power and connectivity subserve motor cortical projections, and how STN-DBS supports them. The effects of ramping STN stimulation on the interaction of motor cortical regions have not been assessed before in the chronic postoperative phase and during fine motor control.

STN-LFP and MEG analysis restricted to the M1 yielded high gamma band (60–90 Hz and 300–400 Hz) peaks increasing with movement and levodopa therapy (86). STN-M1 coherence was also identified in this study in the finely-tuned gamma band (60–90 Hz); it was negatively correlated with clinical symptoms and driven by the STN (86). We note that STN-DBS did not affect the subthalamo-cortical connectivity in the high gamma band (60–100 Hz) comprising the finely-tuned gamma band in our study. A possible mechanism of action of subthalamic stimulation might be that it hampers the pathological beta-driven network inhibition and activates the cortex antidromically through the hyperdirect pathway (147). Our results support this hypothesis, as we observed parallel reductions in high beta hyperdirect connectivity and enhancements in high gamma information processing between the M1 and other motor cortical areas.

Spiral drawing is a complex hand movement that has been less studied concerning the mechanism of action of deep brain stimulation (61, 148). However, analyzing complex movements that require varying degrees of continuous sensory feedback can bring us closer to modeling everyday activities. In Parkinsonian patients, quantitative analysis of spiral drawings has previously shown that linear parameters, including drawing speed, are markers of disease severity (57, 60) and correlate with the motor scores of the Movement Disorder Society-Unified Parkinson's Disease Rating Scale (MDS-UPDRS-III) (57). It may discern early signs of Parkinson's disease with high sensitivity (57). Moreover, spiral testing can objectively monitor the beneficial impact of STN stimulation in the early postoperative phase (61, 148) and react to medication state (59). These findings strengthen the clinical relevance of spiral drawing analysis as an objective marker of motor improvement during DBS therapy.

In our study, tangential velocity increased with ramping stimulation intensity in traced and self-paced spiral drawings. Nonetheless, the entropy of velocity in both tasks only responded to switching stimulation on, not to the gradual increase in stimulation intensity. In a previous study, 2–3 days after DBS electrode insertion, STN-DBS increased spiral drawing velocity during both self-paced and traced spiral drawing tasks, and similarly to our results, patients drew spirals faster during the self-paced drawing task (148). Ramping stimulation intensity in the STN also increased movement speed during repetitive hand movement tasks (28). Dopaminergic substitution (110) and subthalamic stimulation (28, 149) predominantly improved the speed of repetitive hand movements rather than their

amplitude in prior studies. The rhythm reacted the least, and the decrement in speed and amplitude was resistant to both therapies (28, 110, 149), suggesting irregularities in time and space, in accord with our present observation of limited stimulation-induced entropy decrease.

In our study, during both self-paced and traced spiral drawings, ramping STN-DBS decreased low and high beta band power and increased low and high gamma band activity in the motor cortical areas and the subthalamic nucleus in a dose-dependent manner. As a reference, we did not observe stimulation-induced changes in beta and gamma power in the visual cortex on either side. We found these apparent changes only in the tested hemisphere, while the contralateral stimulation was continuously set at the therapeutic level, as in our previous observations with repetitive hand movements (28). These results support the observation that the cortico-subthalamic pathway is strictly ipsilateral (110). We also report that the slope of high beta activity in a subnetwork comprising DLPFC, DPMC, and M1, and the slope of high gamma activity in another subnetwork involving the SMA and M1, predicted the slope of self-paced, but not the traced spiral drawing velocity, during ramping stimulation. It indicates that high beta and high gamma oscillations in networks, including M1, most accurately predict improvement in speed during self-paced spiral drawing. We could not achieve a similar prediction for the traced spiral drawing task, probably because the motor action involved additional areas of the visual and association cortex.

In single-element STN LFP recordings, beta band activity was dominant in the sensorimotor part of the STN, receiving inputs from the primary motor cortex (150). The decrease in low beta activity correlated with alleviation of bradykinesia in the early (99, 151) and chronic (20) postoperative phases. Tinkhauser et al. demonstrated that intraoperative beta band power suppression induced by directional STN-DBS predicted treatment efficacy (152), and it was hypothesized that preservation of motor function may rely on modulation of subthalamic beta LFP activity (153). Prolonged bursting synchronizations of beta oscillations in the subthalamic nucleus correspond to transient yet excessive increases in beta amplitude, and have been linked with impaired motor command and execution in PD (154). The pre-movement timing of subthalamic beta bursts affects movement velocity (155), and the occurrence of beta bursts during movement is associated with speed reduction during self-paced spiral drawing but not

during cued fine motor movements (148). Even the intraburst spike rate positively correlated with bradykinesia and axial scores but not with tremor (145). Bradykinesia alleviation by dopaminergic medication was related to a reduction in beta burst duration in the 13–20 Hz range (151); however, the effect of conventional STN DBS on subthalamic beta burst dynamics remains inconsistent. Intraoperative STN DBS in awake patients did not influence burst rate or duration at rest (156). In contrast, ramping stimulation during repetitive hand movements attenuated beta burst duration (157) and decreased burst amplitude during fine motor control (148) in chronically implanted patients. To clarify the relationship between beta bursts and effective stimulation, comprehensive experimental protocols are needed, recognizing that burst duration, amplitude, and rate are more pronounced in the resting state (148).

Our results indicate that frequency (23, 28) and task-specific (28) subnetwork activity predict bradykinesia severity, in which the M1 and the STN play crucial roles, and that multisensing techniques may point the way forward for the development of adaptive stimulation.

Our results highlight that specific changes in the cortical and subthalamic connections of the primary motor cortex determine the effectiveness of stimulation. Preoperative examination of high gamma effective connectivity between the primary motor cortex and other motor cortical areas, and of high beta hyperdirect connectivity under a levodopa challenge test using EEG, might have predictive value for individual surgical outcomes. Studies using machine learning could further explore these functional and structural network features.

Our study is limited by the disproportionate distribution of male and female patients and the lack of healthy controls. However, the relatively large number of patients included ensures a reliable representation of the statistical sample. The different spirals, namely the traced and self-paced spirals, were drawn only 5 times at each stimulation level. In the future, more trials might further increase the robustness of the statistics. As mentioned earlier, the region-of-interest analyses pipeline in this study included subcortical sources derived from 64-channel EEG data. Although high-density EEG-based source estimation techniques provide an accurate mapping of lateral cortical regions, including the premotor and primary motor cortices, they offer limited sensitivity to mesial cortical and subcortical oscillatory activity. The precise estimation of intrasubthalamic PAC would

require local field potential analysis, considering the anatomical location and small volume of STN (65–155 mm) (158). To optimize the spatial filter source signals, we used the individual T1 and FEM models. We selected the beta and gamma frequency bands, which showed higher signal-to-noise ratios during a motor task with visual feedback, to obtain optimal source signals. Nevertheless, our results must be validated by simultaneous recordings of subthalamic and cortical local field potentials, ensuring accurate tracking of oscillatory dynamics with a higher signal-to-noise ratio.

In conclusion, our study indicates that subthalamic stimulation-reactive high beta hyperdirect activity and high gamma M1-related cortical connections determine changes in bradykinesia during ramping intensity; this underscores the need for a complex multisensing method targeting subthalamic and motor cortical locations to capture symptom-related biomarkers in Parkinson's disease (100).

6. Conclusions

This study demonstrates that STN-DBS exerts frequency-specific effects on the cortico-subthalamic motor network during complex hand movement tasks in patients with Parkinson's disease.

1. STN-DBS reduces abnormal hyperdirect high beta band connectivity between the subthalamic nucleus and motor cortical regions (M1, SMA, DPMC, VPMC), suggesting that the hyperdirect pathway is a key target of DBS.

2. STN-DBS improves communication between cortical motor regions, particularly involving M1, which likely contributes to better motor coordination and clinical improvement by restoring more normal motor network function.

3. Spiral drawing speed improved progressively as stimulation intensity increased, showing a clear dose-dependent improvement in movement execution.

4. Increasing stimulation intensity reduced beta band activity and enhanced gamma oscillations in both the subthalamic nucleus and motor cortical areas, confirming that effective DBS shifts the motor network from pathological beta synchronization toward more physiological gamma activity.

5. High beta and high gamma oscillations in networks, including M1, most accurately predicted the improvement in speed during self-paced spiral drawing, highlighting their value as potential biomarkers of bradykinesia severity and treatment response.

6. These findings suggest that combining subthalamic and cortical signal monitoring could improve adaptive DBS strategies and may help predict individual surgical outcomes. However, larger studies and more detailed protocols are needed to strengthen these findings.

7. Summary

The compound neuronal network dynamics and their relation to improving bradykinesia during bilateral subthalamic nucleus deep brain stimulation (STN-DBS) in Parkinson's disease have not yet been fully explored. Recognition of nervous system biomarkers that reflect everyday symptoms, such as bradykinesia, is a key step toward developing adaptive DBS.

This study investigated how subthalamic nucleus deep brain stimulation changes brain network activity during complex hand movements in patients with Parkinson's disease, focusing on frequency-specific oscillatory patterns linked to bradykinesia. The findings showed that increasing stimulation intensity progressively suppressed abnormal high beta band connectivity (21–30 Hz) between the subthalamic nucleus and motor cortical regions, including the primary motor cortex, supplementary motor area, and premotor cortices. At the same time, STN-DBS enhanced high gamma band information flow between cortical motor areas, suggesting a shift from pathological to more physiological motor network activity.

Increasing stimulation intensity produced dose-dependent increases in spiral drawing speed during both traced and self-paced spiral drawings, accompanied by reductions in beta band and increases in gamma band oscillatory activity within ipsilateral motor cortical and subthalamic networks.

Our findings show that changes in high beta activity within the hyperdirect pathway and high gamma connectivity involving the primary motor cortex are closely linked to improvements in bradykinesia as stimulation intensity increases. Our study is the first to demonstrate that stimulation-induced changes in high beta connectivity along the hyperdirect pathway are bidirectional. These results highlight the importance of monitoring both subthalamic and cortical motor network activity and support the development of integrated multisite sensing approaches to identify reliable, symptom-specific biomarkers in Parkinson's disease.

8. References

1. Li M, Ye X, Huang Z, Ye L, Chen C. Global burden of Parkinson's disease from 1990 to 2021: a population-based study. BMJ Open. 2025;15(4):e095610.

2. Williams D. Why so slow? Models of parkinsonian bradykinesia. Nat Rev Neurosci. 2024;25(8):573–86.

3. Paparella G, De Riggi M, Cannavacciuolo A, Birreci D, Costa D, Angelini L, Alunni Fegatelli D, Fasano A, Espay AJ, Bologna M. Analyzing the 'Bradykinesia Complex' in Parkinson's Disease. Mov Disord. 2026;41(1):143–55.

4. Postuma RB, Berg D, Stern M, Poewe W, Olanow CW, Oertel W, Obeso J, Marek K, Litvan I, Lang AE, Halliday G, Goetz CG, Gasser T, Dubois B, Chan P, Bloem BR, Adler CH, Deuschl G. MDS clinical diagnostic criteria for Parkinson's disease. Mov Disord. 2015;30(12):1591–601.

5. Hughes AJ, Daniel SE, Kilford L, Lees AJ. Accuracy of clinical diagnosis of idiopathic Parkinson's disease: a clinico-pathological study of 100 cases. J Neurol Neurosurg Psychiatry. 1992;55(3):181–4.

6. McIntyre CC, Hahn PJ. Network perspectives on the mechanisms of deep brain stimulation. Neurobiol Dis. 2010;38(3):329–37.

7. Frankemolle-Gilbert AM, Noecker AM, Heida T, McIntyre CC. Comprehensive map of axonal pathway activation as a function of subthalamic deep brain stimulation location and parameter settings. Brain Stimul. 2026;19(1):102992.

8. Bologna M, Paparella G, Fasano A, Hallett M, Berardelli A. Evolving concepts on bradykinesia. Brain. 2020;143(3):727–50.

9. McGregor MM, Nelson AB. Circuit Mechanisms of Parkinson's Disease. Neuron. 2019;101(6):1042–56.

10. Telkes I, Jimenez-Shahed J, Viswanathan A, Abosch A, Ince NF. Prediction of STN-DBS Electrode Implantation Track in Parkinson's Disease by Using Local Field Potentials. Frontiers in Neuroscience. 2016;Volume 10 - 2016.

11. Münte TF, Marco-Pallares J, Heldmann M, Bolat S, Saryyeva A, Müller-Vahl K, Krauss JK. Decoding human response inhibition: evidence from GPi and thalamic electrophysiology during a go/no-go task. Neuroscience. 2025;580:298–305.

12. Muller M, Scafa S, Hanafi I, Varescon C, Palmisano C, van der Gaag S, Zutt R, van der Gaag NA, Hoffmann CFE, Bloch J, Jiménez MC, Bally JF, Capetian P, Isaias IU, Moraud EM, Contarino MF. Online prediction of optimal deep brain stimulation contacts from local field potentials in Parkinson's disease. npj Parkinson's Disease. 2025;11(1):234.

13. Little S, Bonaiuto J, Barnes G, Bestmann S. Human motor cortical beta bursts relate to movement planning and response errors. PLoS Biol. 2019;17(10):e3000479.

14. Mallet N, Pogosyan A, Sharott A, Csicsvari J, Bolam JP, Brown P, Magill PJ. Disrupted dopamine transmission and the emergence of exaggerated beta oscillations in subthalamic nucleus and cerebral cortex. J Neurosci. 2008;28(18):4795–806.

15. Abbasi O, Hirschmann J, Storzer L, Özkurt TE, Elben S, Vesper J, Wojtecki L, Schmitz G, Schnitzler A, Butz M. Unilateral deep brain stimulation suppresses alpha and beta oscillations in sensorimotor cortices. Neuroimage. 2018;174:201–7.

16. Lalo E, Thobois S, Sharott A, Polo G, Mertens P, Pogosyan A, Brown P. Patterns of bidirectional communication between cortex and basal ganglia during movement in patients with Parkinson disease. J Neurosci. 2008;28(12):3008–16.

17. Oswal A, Beudel M, Zrinzo L, Limousin P, Hariz M, Foltynie T, Litvak V, Brown P. Deep brain stimulation modulates synchrony within spatially and spectrally distinct resting state networks in Parkinson's disease. Brain. 2016;139(Pt 5):1482–96.

18. Tinkhauser G, Pogosyan A, Tan H, Herz DM, Kühn AA, Brown P. Beta burst dynamics in Parkinson's disease OFF and ON dopaminergic medication. Brain. 2017;140(11):2968–81.

19. Sharott A, Vinciati F, Nakamura KC, Magill PJ. A Population of Indirect Pathway Striatal Projection Neurons Is Selectively Entrained to Parkinsonian Beta Oscillations. J Neurosci. 2017;37(41):9977–98.

20. Feldmann LK, Lofredi R, Neumann WJ, Al-Fatly B, Roediger J, Bahners BH, Nikolov P, Denison T, Saryyeva A, Krauss JK, Faust K, Florin E, Schnitzler A, Schneider GH, Kühn AA. Toward therapeutic electrophysiology: beta-band suppression as a biomarker in chronic local field potential recordings. NPJ Parkinsons Dis. 2022;8(1):44.

21. Eisinger RS, Cagle JN, Opri E, Alcantara J, Cernera S, Foote KD, Okun MS, Gunduz A. Parkinsonian Beta Dynamics during Rest and Movement in the Dorsal Pallidum and Subthalamic Nucleus. J Neurosci. 2020;40(14):2859–67.

22. Accolla EA, Herrojo Ruiz M, Horn A, Schneider GH, Schmitz-Hübsch T, Draganski B, Kühn AA. Brain networks modulated by subthalamic nucleus deep brain stimulation. Brain. 2016;139(Pt 9):2503–15.

23. Litvak V, Jha A, Eusebio A, Oostenveld R, Foltynie T, Limousin P, Zrinzo L, Hariz MI, Friston K, Brown P. Resting oscillatory cortico-subthalamic connectivity in patients with Parkinson's disease. Brain. 2011;134(Pt 2):359–74.

24. Whitmer D, de Solages C, Hill B, Yu H, Henderson JM, Bronte-Stewart H. High frequency deep brain stimulation attenuates subthalamic and cortical rhythms in Parkinson's disease. Front Hum Neurosci. 2012;6:155.

25. Oswal A, Cao C, Yeh CH, Neumann WJ, Gratwicke J, Akram H, Horn A, Li D, Zhan S, Zhang C, Wang Q, Zrinzo L, Foltynie T, Limousin P, Bogacz R, Sun B, Husain M, Brown P, Litvak V. Neural signatures of hyperdirect pathway activity in Parkinson's disease. Nat Commun. 2021;12(1):5185.

26. Mathiopoulou V, Lofredi R, Feldmann LK, Habets J, Darcy N, Neumann WJ, Faust K, Schneider GH, Kühn AA. Modulation of subthalamic beta oscillations by movement, dopamine, and deep brain stimulation in Parkinson's disease. NPJ Parkinsons Dis. 2024;10(1):77.

27. Mirpour K, Pouratian N. Interaction of motor behaviour, cortical oscillations and deep brain stimulation in Parkinson's disease. Brain. 2025;148(3):886–95.

28. Muthuraman M, Palotai M, Jávor-Duray B, Kelemen A, Koirala N, Halász L, Erőss L, Fekete G, Bognár L, Deuschl G, Tamás G. Frequency-specific network activity predicts bradykinesia severity in Parkinson's disease. Neuroimage Clin. 2021;32:102857.

29. Fischer P, Pogosyan A, Herz DM, Cheeran B, Green AL, Fitzgerald J, Aziz TZ, Hyam J, Little S, Foltynie T, Limousin P, Zrinzo L, Brown P, Tan H. Subthalamic nucleus gamma activity increases not only during movement but also during movement inhibition. Elife. 2017;6.

30. Brücke C, Huebl J, Schönecker T, Neumann WJ, Yarrow K, Kupsch A, Blahak C, Lütjens G, Brown P, Krauss JK, Schneider GH, Kühn AA. Scaling of movement is related to pallidal γ oscillations in patients with dystonia. J Neurosci. 2012;32(3):1008–19.

31. Ulloa JL. The Control of Movements via Motor Gamma Oscillations. Front Hum Neurosci. 2021;15:787157.

32. Anzak A, Gaynor L, Beigi M, Foltynie T, Limousin P, Zrinzo L, Brown P, Jahanshahi M. Subthalamic nucleus gamma oscillations mediate a switch from automatic to controlled processing: a study of random number generation in Parkinson's disease. Neuroimage. 2013;64:284–9.

33. Joundi RA, Jenkinson N, Brittain JS, Aziz TZ, Brown P. Driving oscillatory activity in the human cortex enhances motor performance. Curr Biol. 2012;22(5):403–7.

34. Jenkinson N, Kühn AA, Brown P. γ oscillations in the human basal ganglia. Exp Neurol. 2013;245:72–6.

35. Wiest C, Tinkhauser G, Pogosyan A, He S, Baig F, Morgante F, Mostofi A, Pereira EA, Tan H, Brown P, Torrecillos F. Subthalamic deep brain stimulation induces finely-tuned gamma oscillations in the absence of levodopa. Neurobiol Dis. 2021;152:105287.

36. Piña-Fuentes D, van Dijk JMC, van Zijl JC, Moes HR, van Laar T, Oterdoom DLM, Little S, Brown P, Beudel M. Acute effects of adaptive Deep Brain Stimulation in Parkinson's disease. Brain Stimul. 2020;13(6):1507–16.

37. Wong JK, Middlebrooks EH, Grewal SS, Almeida L, Hess CW, Okun MS. A Comprehensive Review of Brain Connectomics and Imaging to Improve Deep Brain Stimulation Outcomes. Mov Disord. 2020;35(5):741–51.

38. Merola A, Romagnolo A, Krishna V, Pallavaram S, Carcieri S, Goetz S, Mandybur G, Duker AP, Dalm B, Rolston JD, Fasano A, Verhagen L. Current Directions in Deep Brain Stimulation for Parkinson's Disease-Directing Current to Maximize Clinical Benefit. Neurol Ther. 2020;9(1):25–41.

39. Grefkes C, Eickhoff SB, Nowak DA, Dafotakis M, Fink GR. Dynamic intra- and interhemispheric interactions during unilateral and bilateral hand movements assessed with fMRI and DCM. Neuroimage. 2008;41(4):1382–94.

40. Alegre M, Alonso-Frech F, Rodríguez-Oroz MC, Guridi J, Zamarbide I, Valencia M, Manrique M, Obeso JA, Artieda J. Movement-related changes in oscillatory activity in the human subthalamic nucleus: ipsilateral vs. contralateral movements. Eur J Neurosci. 2005;22(9):2315–24.

41. Hirschmann J, Özkurt TE, Butz M, Homburger M, Elben S, Hartmann CJ, Vesper J, Wojtecki L, Schnitzler A. Differential modulation of STN-cortical and cortico-muscular coherence by movement and levodopa in Parkinson's disease. Neuroimage. 2013;68:203–13.

42. Swan BD, Grill WM, Turner DA. Investigation of deep brain stimulation mechanisms during implantable pulse generator replacement surgery. Neuromodulation. 2014;17(5):419–24; discussion 24.

43. The Unified Parkinson's Disease Rating Scale (UPDRS): status and recommendations. Mov Disord. 2003;18(7):738–50.

44. Goetz CG, Tilley BC, Shaftman SR, Stebbins GT, Fahn S, Martinez-Martin P, Poewe W, Sampaio C, Stern MB, Dodel R, Dubois B, Holloway R, Jankovic J,

Kulisevsky J, Lang AE, Lees A, Leurgans S, LeWitt PA, Nyenhuis D, Olanow CW, Rascol O, Schrag A, Teresi JA, van Hilten JJ, LaPelle N. Movement Disorder Society-sponsored revision of the Unified Parkinson's Disease Rating Scale (MDS-UPDRS): scale presentation and clinimetric testing results. Mov Disord. 2008;23(15):2129–70.

45. Evers LJW, Krijthe JH, Meinders MJ, Bloem BR, Heskes TM. Measuring Parkinson's disease over time: The real-world within-subject reliability of the MDS-UPDRS. Mov Disord. 2019;34(10):1480–7.

46. Bologna M, Espay AJ, Fasano A, Paparella G, Hallett M, Berardelli A. Redefining Bradykinesia. Mov Disord. 2023;38(4):551–7.

47. Stebbins GT, Goetz CG. Factor structure of the Unified Parkinson's Disease Rating Scale: Motor Examination section. Mov Disord. 1998;13(4):633–6.

48. Kenny L, Azizi Z, Moore K, Alcock M, Heywood S, Johnson A, McGrath K, Foley MJ, Sweeney B, O'Sullivan S, Barton J, Tedesco S, Sica M, Crowe C, Timmons S. Inter-rater reliability of hand motor function assessment in Parkinson's disease: Impact of clinician training. Clin Park Relat Disord. 2024;11:100278.

49. Heldman DA, Giuffrida JP, Chen R, Payne M, Mazzella F, Duker AP, Sahay A, Kim SJ, Revilla FJ, Espay AJ. The modified bradykinesia rating scale for Parkinson's disease: reliability and comparison with kinematic measures. Mov Disord. 2011;26(10):1859–63.

50. Hasan H, Athauda DS, Foltynie T, Noyce AJ. Technologies Assessing Limb Bradykinesia in Parkinson's Disease. J Parkinsons Dis. 2017;7(1):65–77.

51. Vanhelst J, Béghin L, Duhamel A, Bergman P, Sjöström M, Gottrand F. Comparison of uniaxial and triaxial accelerometry in the assessment of physical activity among adolescents under free-living conditions: the HELENA study. BMC Med Res Methodol. 2012;12:26.

52. Summa S, Tosi J, Taffoni F, Di Biase L, Marano M, Rizzo AC, Tombini M, Di Pino G, Formica D. Assessing bradykinesia in Parkinson's disease using gyroscope signals. IEEE Int Conf Rehabil Robot. 2017;2017:1556–61.

53. Cavazzuti L, Damiano B, Merlo A, Bò MC, Scaltriti S, Cavallieri F, Di Rauso G, Portaro G, Argenziano G, Fioravanti V, Campanini I. The use of single-point magneto-inertial measurement for gait and dynamic balance assessment of patients with Parkinson's disease and Parkinsonisms: a systematic review with critical appraisal of clinical applications and quality of reporting. Front Neurol. 2026;17:1758979.

54. Griffiths RI, Kotschet K, Arfon S, Xu ZM, Johnson W, Drago J, Evans A, Kempster P, Raghav S, Horne MK. Automated assessment of bradykinesia and dyskinesia in Parkinson's disease. J Parkinsons Dis. 2012;2(1):47–55.

55. Goetz CG, Stebbins GT, Wolff D, DeLeeuw W, Bronte-Stewart H, Elble R, Hallett M, Nutt J, Ramig L, Sanger T, Wu AD, Kraus PH, Blasucci LM, Shamim EA, Sethi KD, Spielman J, Kubota K, Grove AS, Dishman E, Taylor CB. Testing objective measures of motor impairment in early Parkinson's disease: Feasibility study of an at-home testing device. Mov Disord. 2009;24(4):551–6.

56. Arora S, Venkataraman V, Zhan A, Donohue S, Biglan KM, Dorsey ER, Little MA. Detecting and monitoring the symptoms of Parkinson's disease using smartphones: A pilot study. Parkinsonism Relat Disord. 2015;21(6):650–3.

57. San Luciano M, Wang C, Ortega RA, Yu Q, Boschung S, Soto-Valencia J, Bressman SB, Lipton RB, Pullman S, Saunders-Pullman R. Digitized Spiral Drawing: A Possible Biomarker for Early Parkinson's Disease. PLoS One. 2016;11(10):e0162799.

58. Saunders-Pullman R, Derby C, Stanley K, Floyd A, Bressman S, Lipton RB, Deligtisch A, Severt L, Yu Q, Kurtis M, Pullman SL. Validity of spiral analysis in early Parkinson's disease. Mov Disord. 2008;23(4):531–7.

59. Danna J, Velay JL, Eusebio A, Véron-Delor L, Witjas T, Azulay JP, Pinto S. Digitalized spiral drawing in Parkinson's disease: A tool for evaluating beyond the written trace. Hum Mov Sci. 2019;65.

60. Zham P, Kumar DK, Dabnichki P, Poosapadi Arjunan S, Raghav S. Distinguishing Different Stages of Parkinson's Disease Using Composite Index of Speed and Pen-Pressure of Sketching a Spiral. Front Neurol. 2017;8:435.

61. Radmard S, Ortega RA, Ford B, Vanegas-Arroyave N, McKhann GM, 2nd, Sheth SA, Winfield L, Luciano MS, Saunders-Pullman R, Pullman SL. Using computerized spiral analysis to evaluate deep brain stimulation outcomes in Parkinson disease. Clin Neurol Neurosurg. 2021;208:106878.

62. Jakobs M, Fomenko A, Lozano AM, Kiening KL. Cellular, molecular, and clinical mechanisms of action of deep brain stimulation-a systematic review on established indications and outlook on future developments. EMBO Mol Med. 2019;11(4).

63. Bronstein JM, Tagliati M, Alterman RL, Lozano AM, Volkmann J, Stefani A, Horak FB, Okun MS, Foote KD, Krack P, Pahwa R, Henderson JM, Hariz MI, Bakay RA, Rezai A, Marks WJ, Jr., Moro E, Vitek JL, Weaver FM, Gross RE, DeLong MR. Deep brain stimulation for Parkinson disease: an expert consensus and review of key issues. Arch Neurol. 2011;68(2):165.

64. Deuschl G, Schade-Brittinger C, Krack P, Volkmann J, Schäfer H, Bötzel K, Daniels C, Deutschländer A, Dillmann U, Eisner W, Gruber D, Hamel W, Herzog J, Hilker R, Klebe S, Kloss M, Koy J, Krause M, Kupsch A, Lorenz D, Lorenzl S, Mehdorn HM, Moringlane JR, Oertel W, Pinsker MO, Reichmann H, Reuss A, Schneider GH, Schnitzler A, Steude U, Sturm V, Timmermann L, Tronnier V, Trottenberg T, Wojtecki L, Wolf E, Poewe W, Voges J. A randomized trial of deep-brain stimulation for Parkinson's disease. N Engl J Med. 2006;355(9):896–908.

65. Schuepbach WM, Rau J, Knudsen K, Volkmann J, Krack P, Timmermann L, Hälbig TD, Hesekamp H, Navarro SM, Meier N, Falk D, Mehdorn M, Paschen S, Maarouf M, Barbe MT, Fink GR, Kupsch A, Gruber D, Schneider GH, Seigneuret E, Kistner A, Chaynes P, Ory-Magne F, Brefel Courbon C, Vesper J, Schnitzler A, Wojtecki L, Houeto JL, Bataille B, Maltête D, Damier P, Raoul S, Sixel-Doering F, Hellwig D, Gharabaghi A, Krüger R, Pinsker MO, Amtage F, Régis JM, Witjas T, Thobois S, Mertens P, Kloss M, Hartmann A, Oertel WH, Post B, Speelman H, Agid Y, Schade-Brittinger C, Deuschl G. Neurostimulation for Parkinson's disease with early motor complications. N Engl J Med. 2013;368(7):610–22.

66. Barbosa RMG, Soares MC, Portela D, Guimarães TG, Cury RG. New Perspectives of Deep Brain Stimulation Indications for Parkinson's Disease: A Critical Review. Brain Sci. 2024;14(7).

67. Antonini A, Stoessl AJ, Kleinman LS, Skalicky AM, Marshall TS, Sail KR, Onuk K, Odin PLA. Developing consensus among movement disorder specialists on clinical indicators for identification and management of advanced Parkinson's disease: a multi-country Delphi-panel approach. Curr Med Res Opin. 2018;34(12):2063–73.

68. Wójcik R, Dębska A, Zaczkowski K, Szmyd B, Podstawka M, Bobeff EJ, Piotrowski M, Ratajczyk P, Jaskólski DJ, Wiśniewski K. Deep Brain Stimulation for Parkinson's Disease-A Narrative Review. Biomedicines. 2025;13(10).

69. Krack P, Batir A, Van Blercom N, Chabardes S, Fraix V, Ardouin C, Koudsie A, Limousin PD, Benazzouz A, LeBas JF, Benabid AL, Pollak P. Five-year follow-up of bilateral stimulation of the subthalamic nucleus in advanced Parkinson's disease. N Engl J Med. 2003;349(20):1925–34.

70. Wakim AA, Mattar JB, Lambert M, Ponce FA. Perioperative complications of deep brain stimulation among patients with advanced age: a single-institution retrospective analysis. J Neurosurg. 2021;135(5):1421–8.

71. Wagle Shukla A, Bange M, Muthuraman M. Patient, target, device, and program selection for DBS in Parkinson's disease: advancing toward precision care. NPJ Parkinsons Dis. 2025;11(1):195.

72. Defer GL, Widner H, Marié RM, Rémy P, Levivier M. Core assessment program for surgical interventional therapies in Parkinson's disease (CAPSIT-PD). Mov Disord. 1999;14(4):572–84.

73. Saranza G, Lang AE. Levodopa challenge test: indications, protocol, and guide. J Neurol. 2021;268(9):3135–43.

74. Okun MS. Deep-brain stimulation for Parkinson's disease. N Engl J Med. 2012;367(16):1529–38.

75. Schlenstedt C, Shalash A, Muthuraman M, Falk D, Witt K, Deuschl G. Effect of high-frequency subthalamic neurostimulation on gait and freezing of gait in Parkinson's disease: a systematic review and meta-analysis. Eur J Neurol. 2017;24(1):18–26.

76. Limousin P, Foltynie T. Long-term outcomes of deep brain stimulation in Parkinson disease. Nat Rev Neurol. 2019;15(4):234–42.

77. Follett KA, Weaver FM, Stern M, Hur K, Harris CL, Luo P, Marks WJ, Jr., Rothlind J, Sagher O, Moy C, Pahwa R, Burchiel K, Hogarth P, Lai EC, Duda JE, Holloway K, Samii A, Horn S, Bronstein JM, Stoner G, Starr PA, Simpson R, Baltuch G, De Salles A, Huang GD, Reda DJ. Pallidal versus subthalamic deep-brain stimulation for Parkinson's disease. N Engl J Med. 2010;362(22):2077–91.

78. Neumann WJ, Steiner LA, Milosevic L. Neurophysiological mechanisms of deep brain stimulation across spatiotemporal resolutions. Brain. 2023;146(11):4456–68.

79. Parent A, Hazrati LN. Functional anatomy of the basal ganglia. II. The place of subthalamic nucleus and external pallidum in basal ganglia circuitry. Brain Res Brain Res Rev. 1995;20(1):128–54.

80. Davidson B, Milosevic L, Kondrataviciute L, Kalia LV, Kalia SK. Neuroscience fundamentals relevant to neuromodulation: Neurobiology of deep brain stimulation in Parkinson's disease. Neurotherapeutics. 2024;21(3):e00348.

81. Einevoll GT, Kayser C, Logothetis NK, Panzeri S. Modelling and analysis of local field potentials for studying the function of cortical circuits. Nat Rev Neurosci. 2013;14(11):770–85.

82. Kahan J, Mancini L, Urner M, Friston K, Hariz M, Holl E, White M, Ruge D, Jahanshahi M, Boertien T, Yousry T, Thornton JS, Limousin P, Zrinzo L, Foltynie T. Therapeutic subthalamic nucleus deep brain stimulation reverses cortico-thalamic coupling during voluntary movements in Parkinson's disease. PLoS One. 2012;7(12):e50270.

83. Crone NE, Miglioretti DL, Gordon B, Lesser RP. Functional mapping of human sensorimotor cortex with electrocorticographic spectral analysis. II. Event-related synchronization in the gamma band. Brain. 1998;121 (Pt 12):2301–15.

84. Rowland NC, De Hemptinne C, Swann NC, Qasim S, Miocinovic S, Ostrem JL, Knight RT, Starr PA. Task-related activity in sensorimotor cortex in Parkinson's disease and essential tremor: changes in beta and gamma bands. Front Hum Neurosci. 2015;9:512.

85. Crowell AL, Ryapolova-Webb ES, Ostrem JL, Galifianakis NB, Shimamoto S, Lim DA, Starr PA. Oscillations in sensorimotor cortex in movement disorders: an electrocorticography study. Brain. 2012;135(Pt 2):615–30.

86. Litvak V, Eusebio A, Jha A, Oostenveld R, Barnes G, Foltynie T, Limousin P, Zrinzo L, Hariz MI, Friston K, Brown P. Movement-related changes in local and long-range synchronization in Parkinson's disease revealed by simultaneous magnetoencephalography and intracranial recordings. J Neurosci. 2012;32(31):10541–53.

87. Swann NC, de Hemptinne C, Thompson MC, Miocinovic S, Miller AM, Gilron R, Ostrem JL, Chizeck HJ, Starr PA. Adaptive deep brain stimulation for Parkinson's disease using motor cortex sensing. J Neural Eng. 2018;15(4):046006.

88. de Hemptinne C, Ryapolova-Webb ES, Air EL, Garcia PA, Miller KJ, Ojemann JG, Ostrem JL, Galifianakis NB, Starr PA. Exaggerated phase-amplitude coupling in the primary motor cortex in Parkinson disease. Proc Natl Acad Sci U S A. 2013;110(12):4780–5.

89. Farokhniaee A, Marceglia S, Priori A, Lowery MM. Effects of Contralateral Deep Brain Stimulation and Levodopa on Subthalamic Nucleus Oscillatory Activity and Phase-Amplitude Coupling. Neuromodulation. 2023;26(2):310–9.

90. Eguchi K, Shirai S, Matsushima M, Kano T, Ichikawa T, Yamazaki K, Hamauchi S, Sasamori T, Seki T, Kitagawa M, Shiraishi H, Houkin K, Sasaki H, Yabe I. Chronic

deep brain stimulation reduces cortical β-γ phase amplitude-coupling in patients with Parkinson's disease. Parkinsonism Relat Disord. 2021;89:148–50.

91. Salimpour Y, Mills KA, Hwang BY, Anderson WS. Phase- targeted stimulation modulates phase-amplitude coupling in the motor cortex of the human brain. Brain Stimul. 2022;15(1):152–63.

92. Lozano AM, Lipsman N, Bergman H, Brown P, Chabardes S, Chang JW, Matthews K, McIntyre CC, Schlaepfer TE, Schulder M, Temel Y, Volkmann J, Krauss JK. Deep brain stimulation: current challenges and future directions. Nat Rev Neurol. 2019;15(3):148–60.

93. Busch JL, Kaplan J, Behnke JK, Witzig VS, Drescher L, Habets JGV, Kühn AA. Chronic adaptive deep brain stimulation for Parkinson's disease: clinical outcomes and programming strategies. NPJ Parkinsons Dis. 2025;11(1):264.

94. Xu H, Wan X, Tu Q, Chen H, Tong M, Xu Z, Cai D. Effect of deep brain stimulation on motor complications in Parkinson's disease: a systematic review and meta-analysis. Front Hum Neurosci. 2025;19:1684229.

95. Chen J, Volkmann J, Ip CW. Author Correction: A framework for translational therapy development in deep brain stimulation. NPJ Parkinsons Dis. 2025;11(1):40.

96. van Wijk BCM, de Bie RMA, Beudel M. A systematic review of local field potential physiomarkers in Parkinson's disease: from clinical correlations to adaptive deep brain stimulation algorithms. J Neurol. 2023;270(2):1162–77.

97. Busch JL, Kaplan J, Habets JGV, Feldmann LK, Roediger J, Köhler RM, Merk T, Faust K, Schneider GH, Bergman H, Neumann WJ, Kühn AA. Single threshold adaptive deep brain stimulation in Parkinson's disease depends on parameter selection, movement state and controllability of subthalamic beta activity. Brain Stimul. 2024;17(1):125–33.

98. Velisar A, Syrkin-Nikolau J, Blumenfeld Z, Trager MH, Afzal MF, Prabhakar V, Bronte-Stewart H. Dual threshold neural closed loop deep brain stimulation in Parkinson disease patients. Brain Stimul. 2019;12(4):868–76.

99. He S, Baig F, Merla A, Torrecillos F, Perera A, Wiest C, Debarros J, Benjaber M, Hart MG, Ricciardi L, Morgante F, Hasegawa H, Samuel M, Edwards M, Denison T, Pogosyan A, Ashkan K, Pereira E, Tan H. Beta-triggered adaptive deep brain stimulation during reaching movement in Parkinson's disease. Brain. 2023;146(12):5015–30.

100. Oehrn CR, Cernera S, Hammer LH, Shcherbakova M, Yao J, Hahn A, Wang S, Ostrem JL, Little S, Starr PA. Chronic adaptive deep brain stimulation versus conventional stimulation in Parkinson's disease: a blinded randomized feasibility trial. Nat Med. 2024;30(11):3345–56.

101. Hentz JG, Mehta SH, Shill HA, Driver-Dunckley E, Beach TG, Adler CH. Simplified conversion method for unified Parkinson's disease rating scale motor examinations. Mov Disord. 2015;30(14):1967–70.

102. Andrade-Souza YM, Schwalb JM, Hamani C, Eltahawy H, Hoque T, Saint-Cyr J, Lozano AM. Comparison of three methods of targeting the subthalamic nucleus for chronic stimulation in Parkinson's disease. Neurosurgery. 2008;62 Suppl 2:875–83.

103. Andrade-Souza YM, Schwalb JM, Hamani C, Eltahawy H, Hoque T, Saint-Cyr J, Lozano AM. Comparison of three methods of targeting the subthalamic nucleus for chronic stimulation in Parkinson's disease. Neurosurgery. 2005;56(2 Suppl):360–8; discussion –8.

104. Neudorfer C, Butenko K, Oxenford S, Rajamani N, Achtzehn J, Goede L, Hollunder B, Ríos AS, Hart L, Tasserie J, Fernando KB, Nguyen TAK, Al-Fatly B, Vissani M, Fox M, Richardson RM, van Rienen U, Kühn AA, Husch AD, Opri E, Dembek T, Li N, Horn A. Lead-DBS v3.0: Mapping deep brain stimulation effects to local anatomy and global networks. Neuroimage. 2023;268:119862.

105. Avants BB, Epstein CL, Grossman M, Gee JC. Symmetric diffeomorphic image registration with cross-correlation: evaluating automated labeling of elderly and neurodegenerative brain. Med Image Anal. 2008;12(1):26–41.

106. Ewert S, Plettig P, Li N, Chakravarty MM, Collins DL, Herrington TM, Kühn AA, Horn A. Toward defining deep brain stimulation targets in MNI space: A subcortical atlas

based on multimodal MRI, histology and structural connectivity. Neuroimage. 2018;170:271–82.

107. Oxenford S, Ríos AS, Hollunder B, Neudorfer C, Boutet A, Elias GJB, Germann J, Loh A, Deeb W, Salvato B, Almeida L, Foote KD, Amaral R, Rosenberg PB, Tang-Wai DF, Wolk DA, Burke AD, Sabbagh MN, Salloway S, Chakravarty MM, Smith GS, Lyketsos CG, Okun MS, Anderson WS, Mari Z, Ponce FA, Lozano A, Neumann WJ, Al-Fatly B, Horn A. WarpDrive: Improving spatial normalization using manual refinements. Med Image Anal. 2024;91:103041.

108. Neumann WJ, Degen K, Schneider GH, Brücke C, Huebl J, Brown P, Kühn AA. Subthalamic synchronized oscillatory activity correlates with motor impairment in patients with Parkinson's disease. Mov Disord. 2016;31(11):1748–51.

109. Vorwerk J, Oostenveld R, Piastra MC, Magyari L, Wolters CH. The FieldTrip-SimBio pipeline for EEG forward solutions. Biomed Eng Online. 2018;17(1):37.

110. Espay AJ, Giuffrida JP, Chen R, Payne M, Mazzella F, Dunn E, Vaughan JE, Duker AP, Sahay A, Kim SJ, Revilla FJ, Heldman DA. Differential response of speed, amplitude, and rhythm to dopaminergic medications in Parkinson's disease. Mov Disord. 2011;26(14):2504–8.

111. Pulliam CL, Heldman DA, Orcutt TH, Mera TO, Giuffrida JP, Vitek JL. Motion sensor strategies for automated optimization of deep brain stimulation in Parkinson's disease. Parkinsonism Relat Disord. 2015;21(4):378–82.

112. Berki Á J, Ding H, Palotai M, Halász L, Erőss L, Fekete G, Bognár L, Barsi P, Kelemen A, Jávor-Duray B, Pichner É, Muthuraman M, Tamás G. Subthalamic stimulation evokes hyperdirect high beta interruption and cortical high gamma entrainment in Parkinson's disease. NPJ Parkinsons Dis. 2025;11(1):95.

113. Haubenberger D, Kalowitz D, Nahab FB, Toro C, Ippolito D, Luckenbaugh DA, Wittevrongel L, Hallett M. Validation of digital spiral analysis as outcome parameter for clinical trials in essential tremor. Mov Disord. 2011;26(11):2073–80.

114. Lee K. Sample Entropy, MATLAB Central File Exchange. 2026 [Available from: https://www.mathworks.com/matlabcentral/fileexchange/35784-sample-entropy.

115. Tadel F, Baillet S, Mosher JC, Pantazis D, Leahy RM. Brainstorm: a user-friendly application for MEG/EEG analysis. Comput Intell Neurosci. 2011;2011:879716.

116. Medani T, Garcia-Prieto J, Tadel F, Antonakakis M, Erdbrügger T, Höltershinken M, Mead W, Schrader S, Joshi A, Engwer C, Wolters CH, Mosher JC, Leahy RM. Brainstorm-DUNEuro: An integrated and user-friendly Finite Element Method for modeling electromagnetic brain activity. Neuroimage. 2023;267:119851.

117. Ashburner J, Friston KJ. Unified segmentation. Neuroimage. 2005;26(3):839–51.

118. Thielscher A, Antunes A, Saturnino GB. Field modeling for transcranial magnetic stimulation: A useful tool to understand the physiological effects of TMS? Annu Int Conf IEEE Eng Med Biol Soc. 2015;2015:222–5.

119. Schrader S, Westhoff A, Piastra MC, Miinalainen T, Pursiainen S, Vorwerk J, Brinck H, Wolters CH, Engwer C. DUNEuro-A software toolbox for forward modeling in bioelectromagnetism. PLoS One. 2021;16(6):e0252431.

120. Van Veen BD, van Drongelen W, Yuchtman M, Suzuki A. Localization of brain electrical activity via linearly constrained minimum variance spatial filtering. IEEE Trans Biomed Eng. 1997;44(9):867–80.

121. Mayka MA, Corcos DM, Leurgans SE, Vaillancourt DE. Three-dimensional locations and boundaries of motor and premotor cortices as defined by functional brain imaging: a meta-analysis. Neuroimage. 2006;31(4):1453–74.

122. Keuken MC, Bazin PL, Schäfer A, Neumann J, Turner R, Forstmann BU. Ultra-high 7T MRI of structural age-related changes of the subthalamic nucleus. J Neurosci. 2013;33(11):4896–900.

123. Lofredi R, Tan H, Neumann WJ, Yeh CH, Schneider GH, Kühn AA, Brown P. Beta bursts during continuous movements accompany the velocity decrement in Parkinson's disease patients. Neurobiol Dis. 2019;127:462–71.

124. Cao CY, Zeng K, Li DY, Zhan SK, Li XL, Sun BM. Modulations on cortical oscillations by subthalamic deep brain stimulation in patients with Parkinson disease: A MEG study. Neurosci Lett. 2017;636:95–100.

125. Baccala LA, Sameshima K, Takahashi DY, editors. Generalized Partial Directed Coherence. 2007 15th International Conference on Digital Signal Processing; 2007 1–4 July 2007.

126. Yang Y, Wei L, Hu Y, Wu Y, Hu L, Nie S. Classification of Parkinson's disease based on multi-modal features and stacking ensemble learning. J Neurosci Methods. 2021;350:109019.

127. Fan R-E, Chen P-H, Lin C-J. Working Set Selection Using Second Order Information for Training Support Vector Machines. Journal of Machine Learning Research. 2005;6:1889–918.

128. Lundberg S, Lee S-I. A Unified Approach to Interpreting Model Predictions2017.

129. Brittain JS, Brown P. Oscillations and the basal ganglia: motor control and beyond. Neuroimage. 2014;85 Pt 2(Pt 2):637–47.

130. Hacker ML, Rajamani N, Neudorfer C, Hollunder B, Oxenford S, Li N, Sternberg AL, Davis TL, Konrad PE, Horn A, Charles D. Connectivity Profile for Subthalamic Nucleus Deep Brain Stimulation in Early Stage Parkinson Disease. Ann Neurol. 2023;94(2):271–84.

131. Horn A, Reich M, Vorwerk J, Li N, Wenzel G, Fang Q, Schmitz-Hübsch T, Nickl R, Kupsch A, Volkmann J, Kühn AA, Fox MD. Connectivity Predicts deep brain stimulation outcome in Parkinson disease. Ann Neurol. 2017;82(1):67–78.

132. Baudrexel S, Witte T, Seifried C, von Wegner F, Beissner F, Klein JC, Steinmetz H, Deichmann R, Roeper J, Hilker R. Resting state fMRI reveals increased subthalamic nucleus-motor cortex connectivity in Parkinson's disease. Neuroimage. 2011;55(4):1728–38.

133. Kahan J, Mancini L, Flandin G, White M, Papadaki A, Thornton J, Yousry T, Zrinzo L, Hariz M, Limousin P, Friston K, Foltynie T. Deep brain stimulation has state-dependent effects on motor connectivity in Parkinson's disease. Brain. 2019;142(8):2417–31.

134. Fogelson N, Williams D, Tijssen M, van Bruggen G, Speelman H, Brown P. Different functional loops between cerebral cortex and the subthalmic area in Parkinson's disease. Cereb Cortex. 2006;16(1):64–75.

135. Williams D, Tijssen M, Van Bruggen G, Bosch A, Insola A, Di Lazzaro V, Mazzone P, Oliviero A, Quartarone A, Speelman H, Brown P. Dopamine-dependent changes in the functional connectivity between basal ganglia and cerebral cortex in humans. Brain. 2002;125(Pt 7):1558–69.

136. Sharott A, Magill PJ, Harnack D, Kupsch A, Meissner W, Brown P. Dopamine depletion increases the power and coherence of beta-oscillations in the cerebral cortex and subthalamic nucleus of the awake rat. Eur J Neurosci. 2005;21(5):1413–22.

137. Jávor-Duray BN, Vinck M, van der Roest M, Mulder AB, Stam CJ, Berendse HW, Voorn P. Early-onset cortico-cortical synchronization in the hemiparkinsonian rat model. J Neurophysiol. 2015;113(3):925–36.

138. Yu Y, Han F, Wang Q. Exploring phase-amplitude coupling from primary motor cortex-basal ganglia-thalamus network model. Neural Netw. 2022;153:130–41.

139. Cohen SL, Woo Choi J, Toga AW, Pouratian N, Duncan D. Exaggerated High-Beta Oscillations are Associated with Cortical Thinning at the Motor Cortex in Parkinson's Disease. Annu Int Conf IEEE Eng Med Biol Soc. 2023;2023:1–4.

140. Sharott A, Magill PJ, Bolam JP, Brown P. Directional analysis of coherent oscillatory field potentials in the cerebral cortex and basal ganglia of the rat. J Physiol. 2005;562(Pt 3):951–63.

141. Jahfari S, Waldorp L, van den Wildenberg WP, Scholte HS, Ridderinkhof KR, Forstmann BU. Effective connectivity reveals important roles for both the hyperdirect

(fronto-subthalamic) and the indirect (fronto-striatal-pallidal) fronto-basal ganglia pathways during response inhibition. J Neurosci. 2011;31(18):6891–9.

142. Bocci T, Ferrara R, Albizzati T, Averna A, Guidetti M, Marceglia S, Priori A. Asymmetries of the subthalamic activity in Parkinson's disease: phase-amplitude coupling among local field potentials. Brain Commun. 2024;6(3):fcae201.

143. Wu T, Long X, Wang L, Hallett M, Zang Y, Li K, Chan P. Functional connectivity of cortical motor areas in the resting state in Parkinson's disease. Hum Brain Mapp. 2011;32(9):1443–57.

144. Conti M, Bovenzi R, Garasto E, Schirinzi T, Placidi F, Mercuri NB, Cerroni R, Pierantozzi M, Stefani A. Brain Functional Connectivity in de novo Parkinson's Disease Patients Based on Clinical EEG. Front Neurol. 2022;13:844745.

145. Sharott A, Gulberti A, Zittel S, Tudor Jones AA, Fickel U, Münchau A, Köppen JA, Gerloff C, Westphal M, Buhmann C, Hamel W, Engel AK, Moll CK. Activity parameters of subthalamic nucleus neurons selectively predict motor symptom severity in Parkinson's disease. J Neurosci. 2014;34(18):6273–85.

146. Wang MB, Boring MJ, Ward MJ, Richardson RM, Ghuman AS. Deep brain stimulation for parkinson's disease induces spontaneous cortical hypersynchrony in extended motor and cognitive networks. Cereb Cortex. 2022;32(20):4480–91.

147. Milosevic L, Kalia SK, Hodaie M, Lozano AM, Fasano A, Popovic MR, Hutchison WD. Neuronal inhibition and synaptic plasticity of basal ganglia neurons in Parkinson's disease. Brain. 2018;141(1):177–90.

148. Bange M, Gonzalez-Escamilla G, Herz DM, Tinkhauser G, Glaser M, Ciolac D, Pogosyan A, Kreis SL, Luhmann HJ, Tan H, Groppa S. Subthalamic stimulation modulates context-dependent effects of beta bursts during fine motor control. Nat Commun. 2024;15(1):3166.

149. Tamás G, Kelemen A, Radics P, Valálik I, Heldman D, Klivényi P, Vécsei L, Hidasi E, Halász L, Kis D, Barsi P, Golopencza P, Erőss L. Effect of subthalamic

stimulation on distal and proximal upper limb movements in Parkinson's disease. Brain Res. 2016;1648(Pt A):438–44.

150. Horn A, Neumann WJ, Degen K, Schneider GH, Kühn AA. Toward an electrophysiological "sweet spot" for deep brain stimulation in the subthalamic nucleus. Hum Brain Mapp. 2017;38(7):3377–90.

151. Lofredi R, Okudzhava L, Irmen F, Brücke C, Huebl J, Krauss JK, Schneider GH, Faust K, Neumann WJ, Kühn AA. Subthalamic beta bursts correlate with dopamine-dependent motor symptoms in 106 Parkinson's patients. NPJ Parkinsons Dis. 2023;9(1):2.

152. Tinkhauser G, Pogosyan A, Debove I, Nowacki A, Shah SA, Seidel K, Tan H, Brittain JS, Petermann K, di Biase L, Oertel M, Pollo C, Brown P, Schuepbach M. Directional local field potentials: A tool to optimize deep brain stimulation. Mov Disord. 2018;33(1):159–64.

153. Bouthour W, Mégevand P, Donoghue J, Lüscher C, Birbaumer N, Krack P. Biomarkers for closed-loop deep brain stimulation in Parkinson disease and beyond. Nat Rev Neurol. 2019;15(6):343–52.

154. Androulidakis AG, Kühn AA, Chen CC, Blomstedt P, Kempf F, Kupsch A, Schneider GH, Doyle L, Dowsey-Limousin P, Hariz MI, Brown P. Dopaminergic therapy promotes lateralized motor activity in the subthalamic area in Parkinson's disease. Brain. 2007;130(Pt 2):457–68.

155. Torrecillos F, Tinkhauser G, Fischer P, Green AL, Aziz TZ, Foltynie T, Limousin P, Zrinzo L, Ashkan K, Brown P, Tan H. Modulation of Beta Bursts in the Subthalamic Nucleus Predicts Motor Performance. J Neurosci. 2018;38(41):8905–17.

156. Schmidt SL, Peters JJ, Turner DA, Grill WM. Continuous deep brain stimulation of the subthalamic nucleus may not modulate beta bursts in patients with Parkinson's disease. Brain Stimul. 2020;13(2):433–43.

157. Kehnemouyi YM, Wilkins KB, Anidi CM, Anderson RW, Afzal MF, Bronte-Stewart HM. Modulation of beta bursts in subthalamic sensorimotor circuits predicts improvement in bradykinesia. Brain. 2021;144(2):473–86.

158. Kolpakwar S, Arora AJ, Pavan S, Kandadai RM, Alugolu R, Saradhi MV, Borgohain R. Volumetric analysis of subthalamic nucleus and red nucleus in patients of advanced Parkinson's disease using SWI sequences. Surg Neurol Int. 2021;12:377.

9. Bibliography of the candidate's publications

Publications on the topic of the present thesis

Berki ÁJ, Ding H, Palotai M, Halász L, Erőss L, Fekete G, Bognár L, Barsi P, Kelemen A, Jávor-Duray B, Pichner É, Muthurman M, Tamás G. Subthalamic stimulation evokes hyperdirect high beta interruption and cortical high gamma entrainment in Parkinson's disease. NPJ Parkinsons Dis. 2025;11(1):95.
IF: 8.2

Other publications

1. Papp AK, Berki ÁJ, Vinnai P, Ajtay A, Bereczki D, Erőss L, Tamás G. Prevalence estimation of essential tremor in Hungary between 2010 and 2020 based on the National Health Insurance Fund Database. Sci Rep. 2025;15(1):28560.
IF: 3.9

2. Takács TT, Magyar-Stang R, Szatmári S, Sipos I, Saftics K, Berki ÁJ, Évin S, Bereczki D, Varga Cs, Nyilas N, Bíró I, Barsi P, Magyar M, Maurovich-Horváth P, Böjti PP, Pásztor M, Szikora I, Nardai S, Gunda B. Workload and clinical impact of MRI-based extension of reperfusion therapy time window in acute ischaemic stroke-a prospective single-centre study. Geroscience. 2025;47(4):6005–13.
IF: 5.4

3. Kiss R-J, Nagy ZA, Szentes Á, Csüdör Á, Máthé A, Makó H, Bomher E, Berki Á J, Gáll Zs, Szilágyi T, Orbán-Kiss K. In vitro modulation of seizure-like activity with beta-cyclodextrin-complexed rufinamide. Acta Marisiensis - Seria Medica. 2024;70(3):135–40.

4. Végh J, Berki ÁJ. Revisiting neural information, computing and linking capacity. Math Biosci Eng. 2023;20(7):12380–403.

5. Takács TT, Berki ÁJ, Böjti PP, Stang R, Fritz-Reunes PA, Schnekenberg L, Siepmann T, Pintér A, Szatmári Sz, Bereczki D, Gunda B. The impact of SARS-CoV-2 infection on the outcome of acute ischemic stroke-A retrospective cohort study. PLoS One. 2023;18(3):e0282045.
IF: 2.9

6. Végh J, Berki ÁJ. On the Role of Speed in Technological and Biological Information Transfer for Computations. Acta Biotheor. 2022;70(4):26.
IF: 1.3

7. Végh J, Berki ÁJ. Towards Generalizing the Information Theory for Neural Communication. Entropy (Basel). 2022;24(8).
IF: 2.7

8. Mihály I, Molnár T, Berki ÁJ, Bod RB, Orbán-Kis K, Gáll Z, Szilágyi T. Short-Term Amygdala Low-Frequency Stimulation Does not Influence Hippocampal Interneuron Changes Observed in the Pilocarpine Model of Epilepsy. Cells. 2021;10(3).
IF: 7.66

9. Mihály I, Orbán-Kis K, Gáll Z, Berki ÁJ, Bod RB, Szilágyi T. Amygdala Low-Frequency Stimulation Reduces Pathological Phase-Amplitude Coupling in the Pilocarpine Model of Epilepsy. Brain Sci. 2020;10(11).
IF: 3.39

10. Berki ÁJ, Benkő Cs, Székely E, Sász ÉI, Vas KE. Incidence of multidrug-resistant bacteria in tracheal secretions from critically ill patients in the intensive care unit. Bulletin of Medical Sciences. 2020;93(2):77–83.

11. Mihály I, Bod RB, Orban-Kis K, Berki ÁJ, Szilagyi T. The Effect of Deep Brain Stimulation on High Frequency Oscillations in a Chronic Epilepsy Model. Bulletin of Medical Sciences. 2020;93(2):63–70.

12. Mihály I, Berki ÁJ, Szilagyi T, Bod RB, Gáll Z, Orban-Kis K. The effect of amygdala low-frequency stimulation on inter-hippocampal connectivity in the pilocarpine model of epilepsy. Acta Medica Marisiensis. 2021;67.

10. Acknowledgments

First and foremost, I would like to express my gratitude to my supervisor, Dr. Gertrúd Tamás, for her guidance and continuous support throughout this scientific journey. I would also like to thank her for taking me into her research group, trusting me, and providing me with the opportunity to work on this project. I could always count on her, and she consistently provided expert insights and placed the advancement of scientific work above all else, making herself available at any time. Her exceptional work ethic and professionalism inspired me the most, shaped my attitude, and kept me on the right track. I learned an incredible amount from her, and her support played a crucial role in my academic development.

My sincere thanks go to Professor Muthuraman Muthuraman, who provided us with immense help in signal processing during the preparation of the manuscript and the revision process. I am grateful to Hao Ding for teaching me the steps of the source analysis technique, power spectral density analysis, and connectivity analysis used in this work. He has helped us overcome technical difficulties on countless occasions. His patience and expertise were essential to completing this project.

I thank Dr. Marcell Palotai, Dr. Borbála Jávor-Duray, Dr. Andrea Kelemen, and Dr. Gertrúd Tamás for screening and examining 40 patients. I also thank Bori for her valuable insights throughout the revision process, and I thank Dr. Éva Pichnier for helping us with spiral drawing analysis.

I would like to extend my sincere thanks to the neurosurgeons, Professor Dr. Lóránd Erőss, Dr. László Halász, Dr. Gábor Fekete, and Professor Dr. László Bognár for their hard work; without them, this research would not have been possible.

I am also grateful to Professor Dr. Dániel Bereczki, Head of the Institute, for giving me the opportunity to work at the Department of Neurology and conduct my research.

I would like to thank the patients for their unwavering patience during the measurements. Last but not least, I thank my wife, mother, and János for their support and for fostering an environment of patience and understanding.